Nanoscale

Cite this: *Nanoscale*, 2011, **3**, 4042

www.rsc.org/nanoscale

FEATURE ARTICLE

# Optical properties of metallic nanoparticles: manipulating light, heat and forces at the nanoscale

**Eduardo A. Coronado,*[a] Ezequiel R. Encina[a] and Fernando D. Stefani*[b]**

***Received 11th July 2011, Accepted 13th August 2011***
**DOI: 10.1039/c1nr10788g**

We present to a general readership an overview of the rich variety of phenomena and applications that arise from the interaction of metallic nanoparticles with light. First, we present the fundamental physics of localized surface plasmon resonances, the most relevant theories and numerical methods, as well as optical detection schemes. Finally, we explain how the localized surface plasmon resonances are currently exploited for the nanoscale manipulation of light, heat and forces in various applications and experimental investigations.



## 1 Introduction

Noble metal nanoparticles (NPs), especially made of Ag and Au, have been attracting a great deal of attention due to their size and shape dependent optical properties which arise from their surface plasmon resonances. The research community has coined the new term "plasmonics" to denominate the interactions of light with nano-structured metals. Strictly speaking, plasmonics is not a new area of research. The scientific investigation began as early as 1899 with theoretical studies by Arnold Sommerfeld[1] and experimental observations of plasmonic effects in light spectra by Robert Wood in 1902.[2] Later that decade, J. C. Maxwell Garnett, and Gustav Mie and G. Beirträge developed theories explaining the light scattering by metallic NPs.[3,4] However, it was not until a number of theoretical studies appeared in the 1950s that a more complete

[a]*INFIQC.CLCM, Departamento de Fisicoquímica, Facultad de Ciencias Químicas, Universidad Nacional de Córdoba, 5000 Córdoba, Argentina. E-mail: coronado@fcq.unc.edu.ar*
[b]*Departamento de Física & Instituto de Física de Buenos Aires (IFIBA, CONICET), Facultad de Ciencias Exactas y Naturales, Universidad de Buenos Aires, Pabellón 1 Ciudad Universitaria, 1428 Buenos Aires, Argentina. E-mail: fernando.stefani@df.uba.ar*

**Eduardo A. Coronado**

*Eduardo A. Coronado received his PhD in 1995 at the National University of Córdoba (UNC), Argentina, for his work on intermolecular energy transfer under the supervision of Prof. J. C. Ferrero. He did postdoctoral work on semiclassical dynamics with Prof. W. H. Miller at the University of California at Berkeley (1999–2000) and later with Prof. G. C. Schatz on modelling optical properties of metal nanoparticles at Northwestern University, Evanston, Illinois (2001). Since 2005 he is Professor and Independent Researcher of CONICET at the Chemical Science Faculty of the UNC. His present activity is mainly focused on theoretical and experimental aspects of plasmonics, including the near and far field optical properties of noble metal nanoparticles, with applications to ultrasensitive spectroscopies.*

**Ezequiel R. Encina**

*Ezequiel Encina (Río Tercero, Argentina, 1981) obtained his Chemistry degree in 2004 at the National University of Córdoba (UNC), Argentina. In 2010 he obtained his PhD from UNC for his work at the Department of Physical Chemistry of the UNC under the direction of Prof. Eduardo Coronado. Currently, he is a CONICET postdoc in the group of Prof. Coronado. His research interests include the design and synthesis of hybrid metal/semiconductor nanostructures and the study of plasmon–exciton interactions in such nanostructures.*

understanding of surface plasmons was reached. Surface plasmon resonances are coherent oscillations of the electrons of a metal in the vicinity of a metal–dielectric interface. For noble metals, the resonant frequencies lie in the middle of the optical spectrum, and therefore surface plasmons interact strongly with light. The foundation for the systematic experimental study was laid in 1968 by Erich Kretschmann and H. Reather[5] and Andreas Otto,[6] who devised methods to excite propagating surface plasmons on thin metallic films by using prisms to couple light into the metal surfaces. In the late 1970s, the technological exploitation of plasmons began with the pioneering discovery by Martin Fleischmann,[7] and Richard P. van Duyne and David L. Jeanmarie[8] of extraordinary enhancements in the Raman scattering of light by molecules attached to a rough silver surface.

In extended metal–dielectric interfaces surface plasmons are propagating dispersive electromagnetic surface waves coupled to the electron gas (plasma) of the conductor metal. In this case they are called surface plasmon polaritons (SPPs).[9,10] The propagation length of SPPs depends on the losses in the metal and typically ranges from less than a micrometre to a few micrometres. In a metallic particle smaller than the propagation length, surface plasmons are confined to the particle geometry. This effect is extremely pronounced in metallic NPs which act as cavity resonators for the surface plasmons.[11,12] For this reason surface plasmon resonances of NPs are called localized surface plasmon resonances (LSPRs) and depend strongly on the exact size and shape of the NP.

More recently there has been a remarkable growing interest in the field of plasmonics caused by: (i) development of new preparation methods for a wide variety of metallic NPs and nanostructures, (ii) availability of instrumentation and techniques for measuring their morphology and architecture with unprecedented levels of resolution, and (iii) the emergence of novel quantitative theoretical tools for simulating and predicting their optical behavior. The synergy between these three aspects leads to a rapid pace of discoveries, which is also evidenced by the increasing number of publications and reviews published in disciplines spreading over physics, chemistry and biology. Plasmonics can be considered an interdisciplinary area of research with great impact due to its potential applications in miniaturized optical devices, sensors, photonic circuits, medical diagnosis and therapeutics.

In this feature article we present to a general readership the LSPRs, and how they determine the optical properties and potential applications of metallic NPs. In Section 2 we give a qualitative description of the LSPR phenomenon and its main characteristics. Section 3 presents the most important analytical and numerical methods to calculate LSPRs. In Section 4 some general trends and features of LSPRs are discussed. In Section 5, we describe the most relevant optical methods to detect metallic NPs. The current capabilities and the theoretical framework that make LSPR powerful tools to manipulate light, heat and forces on the nanoscale are analyzed in Sections 6, 7 and 8, respectively. Finally in Section 9 we give some concluding remarks.

## 2 Polaritons, surface plasmons and localized surface plasmon resonances

When an electromagnetic field propagates in a bulk material medium, charged particles are set in motion. In turn, the moving charges radiate. At the right frequency of the field, an oscillatory mechanical motion of charged particles may be coupled to the electromagnetic field oscillations. In general, these coupled mechanical–electromagnetic waves are called polaritons. If the moving charges are the ions of an ionic crystal, the mechanical movement corresponds to lattice oscillations (phonons) and the polaritons are called phonon-polaritons. In the case of a metal, when a collective motion of the valence free electrons is coupled to the electromagnetic field, a plasmon–polariton is formed. Because the electromagnetic field must have the right frequency and wavelength in order to drive the electrons resonantly, this phenomenon is also called plasmon resonance. Another way to see it is considering that the electron displacement is accompanied by restoring forces exerted by the positive nuclei; the whole system acts as an oscillator whose natural frequencies correspond to the generation of a plasmon–polariton. A particular plasmon polariton that corresponds to the longitudinal motion of electrons at a metal–dielectric interface is called a surface plasmon polariton (SPP). SPPs propagate at the interface as surface bound electromagnetic waves (*i.e.* their intensity is maximal at the interface and decays exponentially into both the metal and the dielectric) with a wavelength shorter than the one of the electromagnetic field in a vacuum, and determined by the dielectric constants of the metal and the dielectric.[9,10] The propagation length of SPPs is determined by the losses in the metal and usually varies from less than a micrometre to a few micrometres.

SPPs may take place in metallic NPs too, but there they cannot propagate freely. Instead, they are confined to the NP geometry, and therefore the resonant conditions depend not only on the metal and the surrounding dielectric but also on the NP exact size and shape, as well as on the polarization of the field with respect to the NP. These plasmon resonances are called localized surface plasmon resonances (LSPRs). Variations of these parameters give

**Fernando D. Stefani**

*Fernando D. Stefani (Buenos Aires, Argentina, 1975) obtained his PhD in 2004 at the Max-Planck-Institute for Polymer Research (MPI-P, Mainz, Germany) under the direction of Prof. W. Knoll. In 2005 he received the Otto-Hahn-Medal of the Max-Planck-Society. From 2004 to 2009 he did postdoctoral stays at the MPI-P and in the group of Prof. Niek van Hulst at Institute of Photonic Sciences (ICFO, Barcelona, Spain), and was a project leader in the group of Prof. Jochen Feldmann at the Ludwig Maximilians Universität (LMU, Munich, Germany). Since 2009 he is an Associate Researcher of CONICET and a Professor of the Physics Department of the University of Buenos Aires (www.nano.df.uba.ar). His research interests include applied nanoscale physics and optics.*

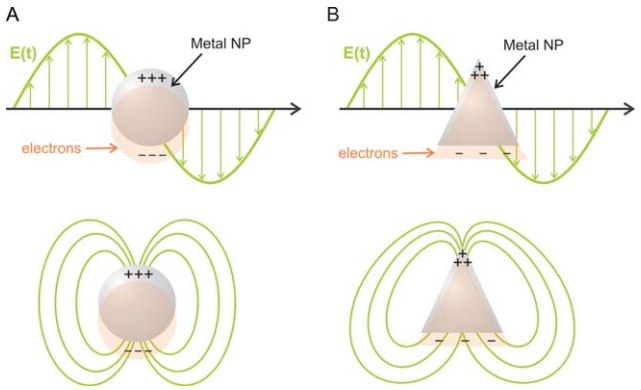


**Fig. 1** Schematic representation of the LSPR of NPs with the shape of a sphere (A) and a triangular prism (B). The electric field shifts the NP conduction electrons from their resting positions around the positive nuclei, which exert a restoring force. The collective movements of electrons are resonant at optical frequencies and the surface charge and local electric field distribution depends on the shape of the NP: in the case of the sphere the field is distributed in a symmetric dipolar pattern, whereas in the case of the triangular NP there is charge and field concentration on the upper tip.

rise to different plasmon modes denoted as dipole, quadrupole, octupole, and $2n^{th}$ multipole, according to the number $n$ of opposite surface charges induced. Each plasmon produces a different surface charge distribution on the NP, and thus a characteristic electric field distribution around the NP. Fig. 1 shows schematically how a time varying electric field would produce different surface charge and electric field distributions on a NP with the shape of a sphere and a triangular prism. While this distinction may be relatively simple in NPs of regular shapes (*e.g.* spheroids or rods), it becomes more complex in NPs with more intricate structures such as branched NPs (*e.g.* nanostars) where the resonances can be described in terms of hybridization between plasmon modes of the different structural components of the NP.[13]

Six fundamental characteristics of LSPRs are crucial to their applications:

### Spectral response

Each LSPR mode has its own eigenfrequency, *i.e.* each mode will interact with a given color of light. The spectral position of a plasmon mode depends on the NP material, size, shape, and on the dielectric properties of the immediate surrounding of the NP.

### Enhanced absorption

Resonant metallic NPs are very efficient light absorbers. At the LSPR frequency, the absorption cross-section may be several times the actual physical cross-section of the NPs.

### Heat generation

Since metallic NPs are very inefficient light emitters, almost all energy absorbed turns into heat. In combination with the enhanced resonant absorption, it is possible to heat different NPs selectively by tuning the color of light to their main LSPR modes.

### Enhanced scattering

The scattering cross-section of a metallic NP is enhanced too at the LSPR frequency. Depending on the NP size, scattering or absorption may dominate. For small NP sizes (roughly below 15 nm) absorption takes over scattering, and the opposite occurs for larger NPs.

### Specific electric field distribution around the NP

Each plasmon mode generates a specific electric field around the NP with two important characteristics. First, it is evanescent, *i.e.* its intensity is maximal at the NP surface and decreases into the surrounding medium with a characteristic decay length of about half the wavelength of the incident light. Second, there are regions (usually called hotspots) where the field intensity is several times stronger than the incident field.

### Directionality

The interaction of a plasmon mode with light has a specific angular pattern. Light will be absorbed or scattered with varying efficiencies depending on the direction. For example, a dipolar LSPR has the typical angular pattern of a dipole. Other LSPR modes may present more complex angular patterns.

The combination of these properties defines the suitability of metallic NPs for applications.

## 3 Theoretical description

In general, a rigorous description of LSPRs requires a multipole expansion of the field inside a NP, so that a superposition of several plasmon modes can be induced at a given frequency. However, for the sake of simplicity it is often assumed that the dominating term in the multipole expansion is the only mode excited. There are a number of analytical as well as numerical methods available to calculate and model the LSPRs of metallic NPs, the details of which have been published in several textbooks and reviews. Here we briefly describe the methods and give reference to more in-depth sources.

For particles of spherical and spheroidal shape, the Mie solutions provide a full analytical model.[14] There are also extensions of the Mie formalism for aggregates of particles.[15] For NPs considerably smaller than the wavelength of light $\lambda$, the Rayleigh (also called dipole or quasi-static) approximation may be applied,[16] which provides useful insight into the physics of LSPRs by means of relatively simple formulae and known parameters. Within this approximation, the polarizability of a small spherical NP is given by:

$$\alpha(\lambda) = 4\pi\varepsilon_0 R^3 \left| \frac{\varepsilon(\lambda) - \varepsilon_m(\lambda)}{\varepsilon(\lambda) + 2\varepsilon_m(\lambda)} \right| \quad (1)$$

where $\varepsilon_0$ is the vacuum permittivity, $R$ is the particle radius, $\varepsilon_m$ and $\varepsilon = \varepsilon' + i\varepsilon''$ are the real relative permittivity of the surrounding medium and the complex relative permittivity of the particle, respectively. The scattering and absorption cross-sections are given by:

$$\sigma_{sca} = \frac{k^4}{6\pi\varepsilon_0^2} |\alpha(\lambda)|^2 \quad (2)$$

$$\sigma_{abs} = \frac{k}{\varepsilon_0} \mathrm{Im}\,[\alpha(\lambda)] \quad (3)$$

The resonance condition in the Rayleigh regime is that $\varepsilon' = -2\varepsilon_m$, *e.g.* the LSPR in air or vacuum occurs at a wavelength $\lambda_{LSPR}$ for which $\varepsilon'(\lambda_{LSPR}) = -2$.

## Numerical methods

Enabled by the computational power of nowadays PCs and computer clusters, numerical methods to solve Maxwell's equations became powerful tools to model NPs and plasmonic devices of arbitrary composition and shape. Some aspects remain challenging and need to be taken into account when using numerical methods. First, some techniques are specific for one type of geometrical configuration. Second, the dielectric constant of metals at optical wavelengths is a complicated complex function of frequency. Thus, several simulation techniques which are limited to lossless, non-dispersive materials are not applicable to plasmonic devices. In addition, in time-domain methods the dispersion properties of metals have to be approximated by suitable analytical expressions. Third, a very fine grid may be required to model evanescent fields at the metal–dielectric interfaces. In fact, most applications of LSPRs are related to sub-wavelength features of the NPs or plasmonic devices, which pose an extra challenge to numerical simulation techniques. Taking these points in mind, we will now give a brief description of some of the most suitable approaches in computational electrodynamics for describing the interaction with light of plasmonic NPs of arbitrary geometry.

**Discrete dipole approximation (DDA).** The NP is represented as a cubic array of $N$ polarizable elements. As one has the freedom to locate these elements of the cubic array at any site, this approximation can be used to model the optical properties of nanostructures of arbitrary shape. The numerical problem is formulated as a set of $N$ linear (complex) non-homogeneous equations which for 3 dimensions takes the shape of a $3N \times 3N$ symmetrical matrix. The dielectric constant of the metal is introduced in the calculation by means of the polarizabilities. The explicit formula for them has been developed by Draine and Goodman[17,18] in such a way that the cubic array of dipoles reproduced the dielectric response of the extended solid to the electromagnetic radiation (lattice dispersion relation). Usually 3D DDA calculations require less computational effort than finite differencing methods. This feature has made the DDA approach a powerful tool to model the optical properties of particles of different shapes and with dimensions of the order of a few hundred nanometres including studies of triangular prisms,[19] cubes,[20] truncated tetrahedral,[21] shell shaped particles,[22] disks[23] and rods,[24] among others.[25]

Although DDA is not an exact method, comparisons of DDA results with other methods such as the Mie theory indicate that errors in the extinction spectra are often less than 10%. There exist several DDA implementations,[26] extensions to periodic targets[27] and light scattering problems on particles placed on surfaces.[28] Comparisons to exact techniques have been published,[29] the validity criteria of the DDA have been recently extended for irregularly shaped particles.[30] A convergence criterion for a precise calculation of the near field using DDA has also been recently proposed.[31]

**Green dyadic methods (GDM).** These methods are based on discretization of an integral equation to obtain a matrix equation. The magnetic field is eliminated from Maxwell's equations, and the field scattered by the object is calculated as the response of the reference system to a point current source by means of the so-called Green's function. The Green's function is a dyad that operates on a vector giving rise to another vector. The GDM is particularly efficient in modeling scattering from metallic structures embedded in uniform or planar layered media. This is due to the fact that Green's functions are available for such systems and only the metallic structure volume has to be discretized. However, it is hard to use the GDM in more general problems due to the difficulty in constructing the related Green's functions. The GDM is a frequency-domain technique, so it can treat arbitrary material dispersion. A very fine grid resolution is required to accurately model the rapid field decay inside the metal. In addition, assuming that an orthogonal grid is used, finer grid resolutions are required for curved metal–dielectric interfaces to avoid introducing large errors due to staircasing.[32] The efficiency of discretization can be increased by using non-uniform and/or non-orthogonal grids.[32,33] These, however, are at the cost of higher complexity codes. It has been shown that the GDM is equivalent to DDA in the low-frequency limit.[18]

**Finite-difference time-domain method (FDTD).** This approach can be classified within the grid-based differential time domain numerical methods, in which the time dependent Maxwell's equations in their partial differential form are discretized using central difference approximations to the space and time partial derivatives. The finite difference equations are solved in a leap-frog way: the components of the electric field in a given space volume are solved at some instant in time, then the components of the magnetic field are solved for the next instant of time. This process is repeated until the desired transient or steady state electromagnetic field behavior has fully evolved. The basic FDTD space grid and time-stepping algorithm traces back to a seminal 1966 paper by Yee.[34] The descriptor "finite-difference time-domain" and its corresponding "FDTD" acronym were originated by Taflove.[35] FDTD is accurate and robust. Its sources of error are well known, and can be restricted to permit accurate models for a very large variety of electromagnetic wave interaction problems.

All the numerical methods discussed can be applied to capriciously complex geometries and frequency dependent dielectric functions, although FDTD requires the permittivity to be expressed as a sum over a limited number of Lorentzians, so it could be difficult to apply to arbitrary intricate dielectric functions. The DDA and FDTD methods rely on simple volume parameterizations, which can be advantageous when very complex geometries are considered. One advantage of the DDA method is that it can be applied to closely separated particles without any need to parameterize the medium between them, whereas FDTD could become prohibitively time consuming for this particular case. On the other hand in contrast to the time independent approaches, the FDTD method relies on the propagation of the electromagnetic field defined on a spatial grid

through consecutive time steps, so the method yields $\boldsymbol{E}(\boldsymbol{r},t)$ in a direct way. This can be advantageous in situations where the time resolved fields are required. FDTD deals with impulsive behavior naturally. A single FDTD simulation can provide either ultra wideband temporal waveforms or the sinusoidal steady-state response at any frequency within the excitation spectrum. It is relatively simple to combine FDTD with sets of auxiliary differential equations that describe other physical phenomena of a complex system (*i.e.* multiphysics solutions). FDTD is a systematic approach. Specifying a new structure in FDTD consists simply of mesh generation problem rather than the potentially complex reformulation of an integral equation (*e.g.* no calculation of structure-dependent Green functions is needed). These factors tend to indicate that FDTD will likely to remain one of the most widely used, and may become the dominant computational electrodynamics technique.[36]

## 4 Some general trends and features of LSPRs

By means of examples of applications of the numerical and analytical approaches we illustrate the general trends on the behavior of LSPRs of different NPs.

### Spheres

Fig. 2 shows the extinction spectra, including the relative contributions of absorption and scattering, of silver nanospheres with increasing diameters. Small spheres whose size is within 1–2% of the incident wavelength (*e.g.* 10 nm Ag as in Fig. 1a) present a single LSPR corresponding to the dipolar resonance and the extinction is dominated by absorption. In this size range the quasistatic approach is valid and the resonant absorption and scattering are given by eqn (2) and (3). As the NP radius ($R$) increases the relative contribution of scattering to the total extinction increases, as expected from the $R^6$ and $R^3$ dependencies of the scattering and absorption cross-sections, respectively (eqn (2) and (3)). Note that the quasistatic approximation does not take into account any size dependence of the spectral position of the LSPR. However, as the size of the particle increases, so does dynamic depolarization which leads to a red-shift and broadening of the LSPR. The dipolar LSPR changes from 354 to 368 and to 466 nm when the size of the Ag spheres increases from 10 to 50 and 100 nm (Fig. 2A–C, respectively). The correct description of spheres larger than about 5% of the wavelength requires the full Mie solution. For even larger particles higher order multipole resonances become significant as shown in Fig. 2C for the 100 nm Ag sphere.

The relative contribution of each multipole order to the total extinction cross-section of a 200 nm diameter silver sphere can be seen in Fig. 3A. The peaks at short wavelengths in the extinction spectra correspond to the quadrupole and octupole excitation, while the broader band at longer wavelengths is due to the dipole excitation. This is clearly seen in the electric field around the NP obtained when it is illuminated at the resonant frequency of each mode. Fig. 3B–D show the electric field around the NP normalized to the incident field ($|E|/|E_0|$). The field corresponding to the dipole mode (Fig. 3B) presents two lobes, while the quadrupole (Fig. 3C) exhibits four lobes. Due to the large spectral overlap with the dipole mode, both quadrupole and dipole are excited simultaneously and the enhancement is not symmetrical having larger enhancements on the right side (where the dipole has its major contribution). The enhancement pattern at the octupole resonance wavelength (Fig. 3D) is almost identical to that of the quadrupole. In this case the contribution to the extinction of this mode is very small compared to the dipole and quadrupole modes, being the field distribution dominated by the other two modes.

In the quasistatic regime the resonance condition for an arbitrary order $j$ is given by $\varepsilon' = -(j + 1)/j$, which means for example that the quadrupole ($j = 2$) and octupole ($j = 3$) LSPRs of a particle in vacuum occur when $\varepsilon'$ is equal to $-1.5$ and $-1.33$, respectively. As the size of the particle increases beyond the quasistatic regime, the higher order resonances red-shift too. A useful way to condense the size dependency of the LSPRs is to evaluate the real part of the dielectric constant $\varepsilon'$ at the resonance wavelength as a function of the sphere diameter, for each multipole order, as depicted in Fig. 4 based on Mie calculations. The values of $\varepsilon'$ for the LSPR are close to the quasistatic value of $-2$ for small sphere diameters in vacuum but increase quickly with size, deviating considerably from this value for radius greater than 25 nm. The rate of variation $\varepsilon'$ decreases with the multipole order, which implies that the shift of the resonance wavelength with size is smaller for the higher order multipoles.

### Rods

In contrast to the case of spheres where the different multipole modes overlap considerably, the longitudinal LSPR modes of

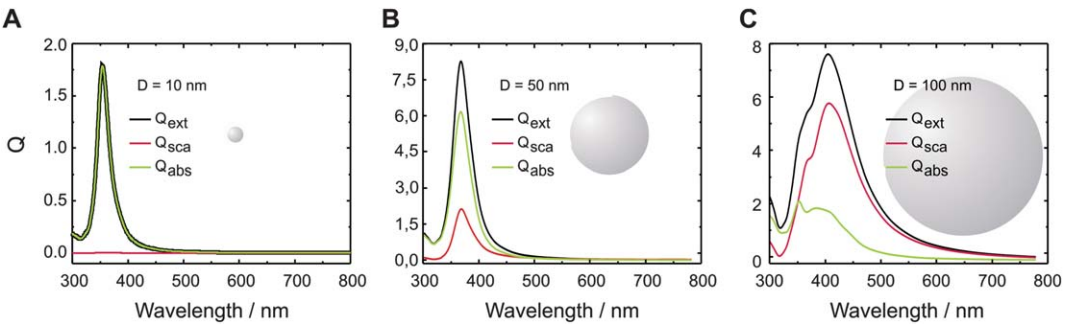


**Fig. 2** Extinction, absorption and scattering efficiencies ($Q$) of spherical silver NPs (in vacuum) with increasing diameter ($D$). The respective efficiencies $Q$ are defined as the ratio between the corresponding cross-section $\sigma$ and the geometrical cross-sectional area of the sphere projected.

 

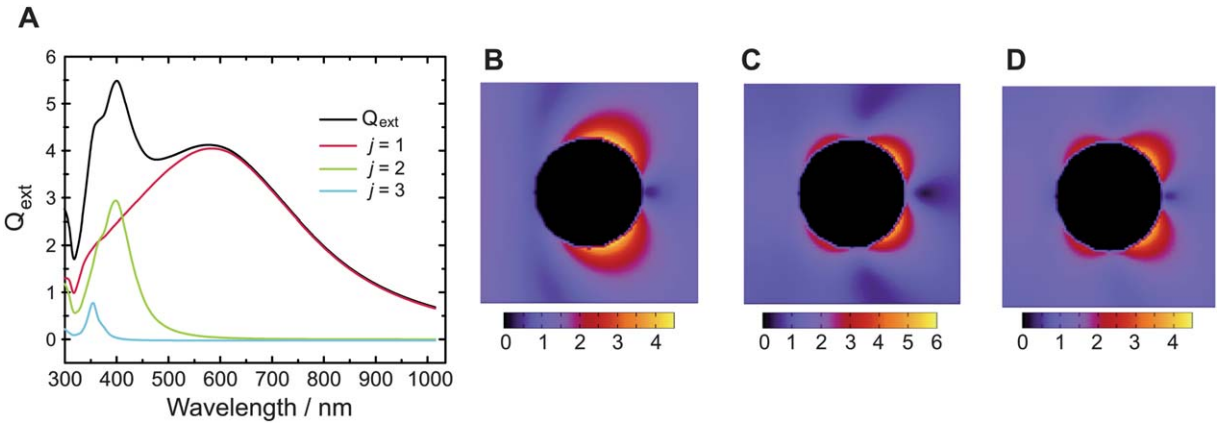


**Fig. 3** LSPR modes of a metallic sphere. (A) Relative contributions of each multipole order ($j$) to the total extinction efficiency of a 200 nm Ag sphere in vacuum. (B, C, and D) Electric field intensity distribution around the NP corresponding to $j = 1, 2, 3$, respectively, when the NP is illuminated from the left with a plane wave at the resonant wavelength of each mode.

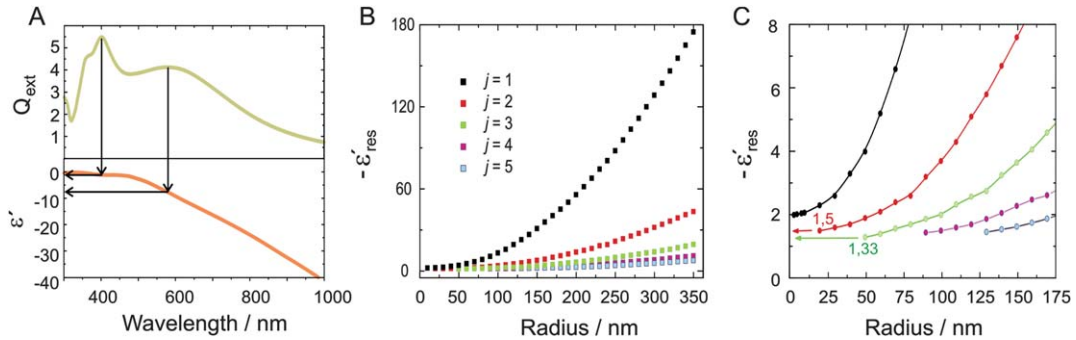


**Fig. 4** Size dependence of the spectral position of the LSPR modes of a spherical NP. (A) The resonances are identified from the extinction spectrum, and the corresponding value of the real part of the dielectric constant $\varepsilon'$ is identified. (B) $\varepsilon'$ for different multipole plasmon modes of silver spheres of increasing radius. (C) A zoom view of (B) to show the asymptotic values of $\varepsilon'$ for small spheres in the quasistatic regime.

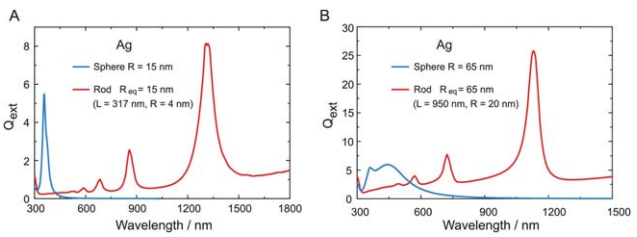


**Fig. 5** Comparison between the LSPR modes of a nanosphere and a nanorod (longitudinal polarization). (A) Extinction spectra of the Ag sphere with radius $R = 15$ nm and a Ag nanorod of equivalent volume. (B) Idem for a sphere with radius $R = 65$ nm. The calculations were performed using DDA for cylinders and Mie solutions for the spheres.

nanorods are well separated spectrally. Fig. 5 shows the extinction spectra of two Ag nanorods of different length and, as reference, of two spheres of equivalent volume. Each peak on the extinction spectra is associated with the excitation of odd LSPR modes, *i.e.* dipole ($j = 1$), octupole ($j = 3$), *etc.* The peak wavelength decreases with increasing plasmon order, being the more redshifted resonance the one corresponding to the dipole mode in this case. These features have been observed experimentally for gold nanorods fabricated using alumina templates.[24] The spectral position of any order LSPR of nanorods can be determined by means of a general resonance condition:[37]

$$\mathrm{Re}[\varepsilon(\lambda)] = \left[\frac{A}{Q^2} + \frac{B}{Q^2 d^2} + C\right]\varepsilon_{\mathrm{m}}(\lambda) \qquad (4)$$

where $A = 2687\ \mu\mathrm{m}^{-2}$, $B = 4.4$ and $C = 3.7$ and $Q = j\pi/L$ are the wavevector associated with the multipole plasmon mode of order $j$ of a gold or silver nanorod of length $L$ and diameter $d$ with dielectric constant $\varepsilon(\lambda)$ in a surrounding medium with dielectric constant $\varepsilon_{\mathrm{m}}(\lambda)$. The expression has been derived combining DDA electrodynamics simulations with the aid of a nanoantenna-standing wave model approach. Some scaling laws, emerging from the above expression, have been also demonstrated to be in very good agreement with recent experiments and theoretical studies.[38–40]

A comparison between two electromagnetic methods, the DDA approach (performed by us) and GDM calculations performed by Krenn *et al.*,[41] is shown in Fig. 6 for nanowires of a rectangular cross-section (25 nm × 85 nm) for different lengths, fabricated by electron beam lithography. The spectra (not shown, similar to the ones shown in Fig. 5) present the well separated LSPR peaks corresponding to modes of different multipole orders. The DDA reproduces the experimental results more accurately.

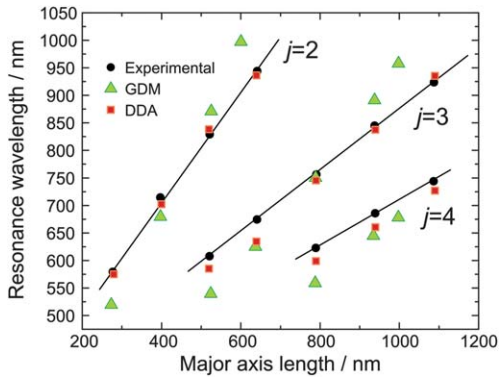


**Fig. 6** Spectral positions of the LSPR modes of the order *j* for nanorods of various lengths with a rectangular cross-section (25 nm × 85 nm). Comparison between the experimental values[41] and numerical simulations performed using DDA and GDM.

### Other NP shapes

Besides nanospheres and nanorods, important efforts have been performed in order to develop chemical and physical methods able to produce other NP shapes. It has been possible to obtain various nanostructures such as nanostars,[42,43] nanocages,[44] nanocubes,[45] nanotriangles[46] and nanoshells[47] with high quality. They present a large variety of LSPR modes, more or less complex depending on the NP geometry, and spanning from the visible to the NIR, which are pertinent to applications in biochemical sensors, in surface enhanced spectroscopies, and photothermal cancer therapy.

### Plasmonic coupling

When two or more NPs are in close vicinity, the localized particle plasmons of the individual NPs interact with each other *via* their optical near fields, creating coupled LSPR modes.[48–50] The resonant frequencies of coupled NPs depend strongly on the interparticle distance and configuration, showing large spectral shifts (in general red-shifts) with respect to the localized particle plasmons of the individual NPs.[48,50–54] In addition their associated electric fields are stronger and more localized in the gaps between the particles.[33,55–59] In Fig. 7A and B the electric field enhancement ($|E|/|E_0|$) pattern generated around a single 25 nm silver NP is compared to the one generated around a dimer of 25 nm Ag NPs separated by a 5 nm gap. The hot spot effect, *i.e.* the enormous enhancement produced as a consequence of near field coupling between NPs, is clearly evidenced. Fig. 7C shows a comparison of the spectra of the single and coupled NPs.

The dependence of the coupled LSPR frequency on the interparticle distance has been used as a "plasmonic ruler" to measure nanometric distances in biological systems.[60,54] For Au NPs, this spectral shift seems to exhibit a universal scaling behavior that is independent of the particle size but not its shape.[61,62] Recently a general plasmon ruler equation for Ag nanosphere pairs has been derived for a wide range of interparticle separations and diameters which demonstrates the importance of including multipole interactions for small interparticle separations.[63]

## 5 Optical detection of metallic NPs

There are numerous methods to detect and characterize metallic NPs. Non-optical methods include scanning probe and electron microscopies. In colloidal suspension, metallic NPs can be studied optically by means of UV-VIS extinction spectroscopy as well as by dynamic light scattering. Near field scanning optical microscopy can be used successfully to investigate metallic NPs, even at the single NP level. However, practical application has been limited by its highly demanding experimental realization. Here, we describe the most successful far-field microscopy methods with capability to address single metallic NPs.

### Dark field detection of NPs

Traditional methods for the far-field optical detection of small objects rely on scattering. The signal is obtained by separating the light elastically scattered by the object from the incident field, *e.g.* as in dark-field or total-internal-reflection microscopy. Indeed these methods can be used to detect NPs. The scattering cross-section of a spherical particle much smaller than the wavelength of light $\lambda$ is given by eqn (2). A key feature of this equation is that the intensity of scattered light scales as the sixth power of the particle diameter $D$, *i.e.* the scattering signal of a particle with $D = 10$ nm, is 1 000 000 times weaker than that of a particle with $D = 100$ nm. Detection of small particles becomes extremely challenging, particularly in complex environments, because one needs to distinguish the light elastically scattered by the particle from stray background scattering produced by any slight fluctuation in the refractive index of the sample. This is

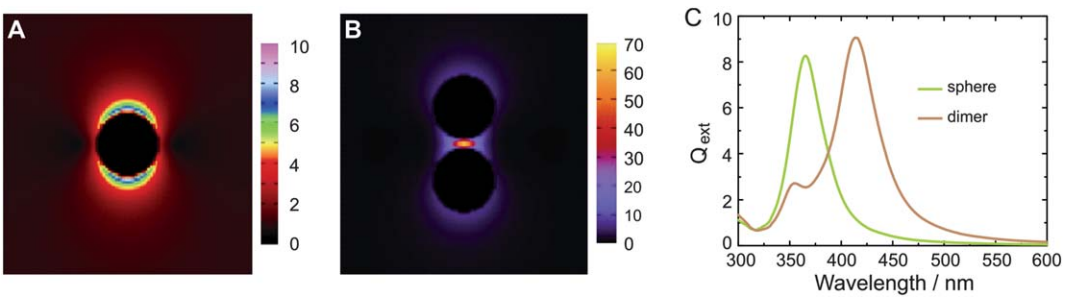


**Fig. 7** Plasmonic coupling. (A, B) Near field enhancement distribution produced by a silver spherical NP with $D = 25$ nm and by a pair of spherical NPs of the same diameter separated by 5 nm, respectively. The incident field is polarized along the major axis (vertically). (C) Spectra of the single spherical NP and the NP pair shown in A and B. The calculations were performed using Generalized Multiparticle Mie Theory.

 

a fundamentally different situation than that of detecting fluorescence, which can be separated from the background efficiently by using spectral filters. Nevertheless, if the scattering efficiency is sufficiently large, it is possible to detect relatively small particles. Metallic NPs are the most prominent example because they exhibit a greatly enhanced scattering in the visible range due to their LSPRs. Their scattering cross-sections may exceed several times their geometrical cross-sections. Gold and silver NPs down to 30–40 nm can be detected by dark-field or total internal reflection microscopy.[64–68]

Fig. 8 shows a schematic of a typical dark-field microscope and a scattering image of individual gold NPs.[69] Optical detection of metallic NPs based on scattering has found important applications in nano- and life-sciences.[54,70–77]

### Interferometric scattering detection

Recently, efforts have been undertaken to detect optically very small metallic NPs ($D < 20$) in order to expand their applicability as labels in the life-sciences and as building blocks in nanotechnology. A few techniques have succeeded. They are all interferometric measurements and thus require coherent (laser) light sources. The signals are produced by scattering or absorption by the particles.

The techniques based on scattering exploit the interference between the background reflection as a reference beam and the field scattered by the NP (Fig. 9).[78–80] In this case, the measured signal $I_m$ is given by the coherent superposition of the scattered and reflected laser fields, $E_s$ and $E_r$, respectively:

$$I_m = |E_r + E_s|^2 = |E_i|^2(r^2 + s^2 - 2|r||s|\sin\varphi) \quad (5)$$

where $E_i$ is the incident field, $r$ is the reflectivity and $s = |s|e^{i\varphi}$ is the complex scattering amplitude with phase $\varphi$. The first term on the right is the reflected background intensity. The second term is the scattered intensity, proportional to $D^6$ and thus is negligible for very small particles. The third term, however, is proportional to $D^3$ and overwhelms the other two terms for very small particles.[78] This method can be applied in wide field mode.[79] Although the resonant response of the metallic particles can be used in some cases to distinguish them from a scattering background, the application of this technique in highly scattering media such as biological cells seems limited.[79]

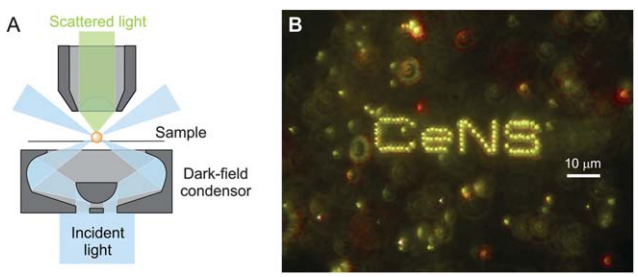


**Fig. 8** Dark-field optical microscopy of metallic NPs. (A) Schematic of a dark-field set-up for the detection of NPs by scattering. (B) Dark-field image of a substrate patterned with gold NPs of $D = 80$ nm by laser printing (from Urban *et al.*[69]). Other NPs free in the colloidal suspension can be seen (slightly out of focus) around the "CeNS" pattern. NP clusters, recognizable by their red color due to plasmonic coupling, can be seen too.

### Direct absorption detection

The techniques that rely on absorption benefit from the fact that absorption scales as $D^3$ in contrast to the $D^6$ dependency of the scattering cross-section. Near their plasmon resonance, metallic NPs have a relatively large absorption cross-section ($\sim 6 \times 10^{-14}$ cm$^2$ for a 5 nm gold NP) and exhibit a fast electron–phonon relaxation in the picoseconds range,[81] which makes them very efficient light absorbers. Thus, for very small NPs techniques based on light absorption become more sensitive than scattering techniques. The absorption signals are still weak and it is necessary to apply some kind of modulation and lock-in amplification in order to detect them efficiently. One possibility is to directly monitor the fluctuations in transmitted light as the position of the absorbing NP is modulated over the focus of the illuminating beam.[82] Gold particles down to 5 nm were detected with this method.[82]

### Photothermal detection

Photothermal techniques exploit the strong absorption of small NPs to generate a simpler to detect scattering signal, by means of the thermal lens effect[83,84] (*i.e.* the dependence of the refractive index with temperature). The luminescence efficiency of the metallic NPs is very low.[85,86] Almost all the light absorbed by a NP is converted into heat and, as a consequence, the temperature of the medium around the NP increases and its index of refraction decreases. Effectively, the heated volume around the NP acts as a scatterer which can be strong enough to be detected in a scanning microscope. Further, the laser induced scattering can be easily switched on and off simply by modulating the intensity of the light used for heating, which in turn enables highly sensitive lock-in detection.

A number of methods have been developed based on this concept. Gold NPs as small as 5 nm in diameter could be detected by a photothermal interference contrast (PIC) method[87] that uses two (reference and probe) spatially separated beams. More recently, a simpler technique where reference and probe beams are collinearly aligned (Fig. 10) has proven to be the most effective method to date permitting the imaging of gold NPs as small as 1.4 nm in diameter (only 65 atoms!).[83]

## 6 Manipulating light at the nanoscale

In this section we focus on the near field distribution of LSPRs and how they can be used to manipulate light at the nanoscale and enable a number of applications. All applications are based on the six fundamental properties presented in Section 2, but first we introduce the important concept of reciprocity in optics that is also relevant to the plasmon resonances of metallic NPs.

### Reciprocity

Roughly, the reciprocity theorem states that the relationship between an oscillating current and the resulting electric field is unaffected if one interchanges the points where the current is placed and where the field is measured. Consider an electric

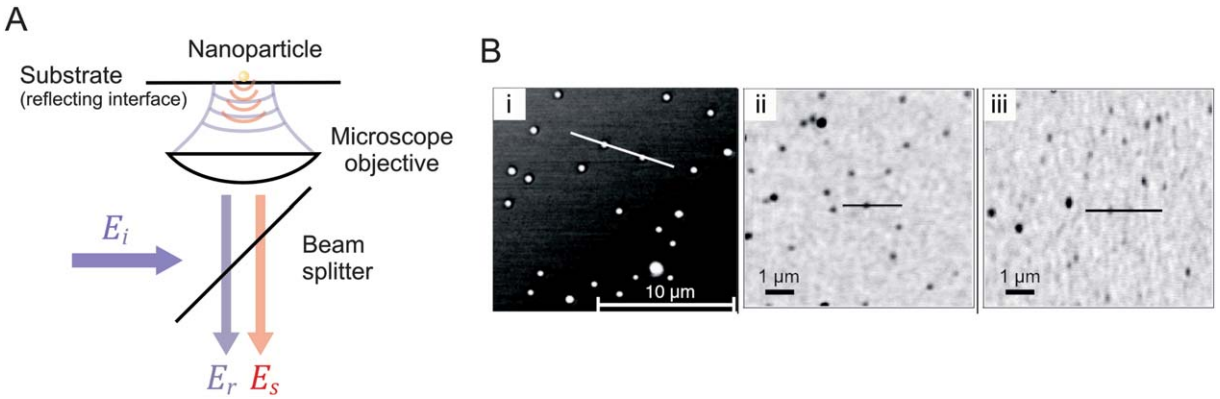


**Fig. 9** Interferometric optical detection of metal NPs. (A) Schematic of the experimental configuration. The sample is scanned over the focus of a confocal microscope. Images are the result of the coherent superposition of the reflected and scattered fields, $E_r$ and $E_s$, respectively (eqn (5)). (B) Confocal interferometric images of samples with gold NPs of different sizes from Sandoghdar *et al.*:[78,79] (i) 60 nm gold NPs.[78] For these relatively large particles the reflective (first) term in eqn (5) dominates and the signal is positive. (ii) Image of a sample with 10 nm and (iii) with 5 nm gold NPs.[79] For these small particles, the interference (third) term of eqn (5) dominates, so the signal is negative.

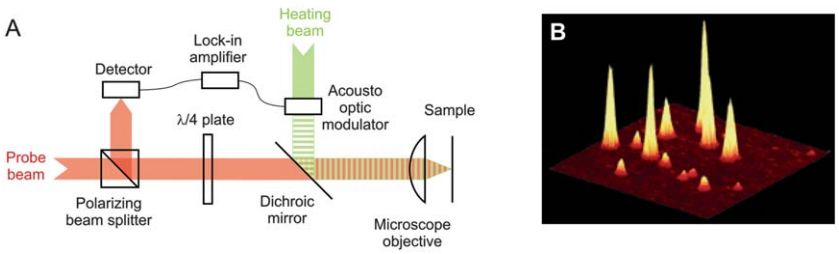


**Fig. 10** Photothermal heterodyne imaging (PHI). (A) Experimental configuration and (B) PHI image from Cognet *et al.*[84] of a sample containing gold NPs with diameters of 5 nm (large peaks) and 2 nm (small peaks).

point-dipole source $\boldsymbol{p}_1$ located at position $\boldsymbol{r}_1$ in a certain medium, producing an electric field $\boldsymbol{E}_1(\boldsymbol{r}_2)$ at another point $\boldsymbol{r}_2$ as depicted in Fig. 11A. Now, consider the situation where source and observation positions are switched, *i.e.* we now have a dipole source $\boldsymbol{p}_2$ (different from $\boldsymbol{p}_1$) at $\boldsymbol{r}_2$ and observe the field $\boldsymbol{E}_2(\boldsymbol{r}_1)$ produced at $\boldsymbol{r}_1$ as in Fig. 11B. The optical reciprocity theorem states that:

$$\boldsymbol{p}_1\boldsymbol{E}_2(\boldsymbol{r}_1) = \boldsymbol{p}_2\boldsymbol{E}_1(\boldsymbol{r}_2) \quad (6)$$

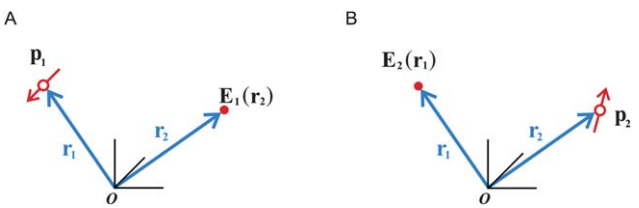


**Fig. 11** (A and B) Reciprocal configurations of dipoles and generated electric fields.

Optical reciprocity is valid in most situations. Actually, reciprocity failures are special cases where the susceptibility tensors are not symmetric, as in the case of magnetic materials in the presence of magnetic fields.[88–90] This simple relation is of great help when studying the interaction of molecules or emitters with plasmonic structures.[91–98] One way to exploit reciprocity is to consider one of the dipoles, let's say $\boldsymbol{p}_1$ in the far field, producing a plane wave, polarized along the direction of $\boldsymbol{p}_1$ and incident on the plasmonic structure (*e.g.* a single or a set of metallic NPs) from a certain direction $\boldsymbol{d}$. That plane wave generates a certain electric field $\boldsymbol{E}_1$ around the plasmonic structure. If we now place the second dipole $\boldsymbol{p}_2$ at $\boldsymbol{r}_2$ near the plasmonic structure, it will interact with the component of the local electric field along the orientation of $\boldsymbol{p}_2$, that is, the right term in eqn (6). The reciprocity theorem tells us that if that interaction is strong, *i.e.* the component of $\boldsymbol{E}_1$ at $\boldsymbol{r}_2$ along the orientation of $\boldsymbol{p}_2$ is large, the emission of $\boldsymbol{p}_2$ into the far field, polarized along the orientation of $\boldsymbol{p}_1$ in the opposite direction $-\boldsymbol{d}$, will be proportionally strong.

This statement is of wide applicability because most molecular transitions, such as fluorescence or Raman, correspond to dipolar excitations; more complex excitations or currents can be described as a superposition of dipoles. Plasmonic NPs may influence optical transitions in the excitation as well as in the emission process. In addition, it clearly states the directionality of plasmonic enhancements which is of critical importance in microscopy and optical antennas.[93] In summary, one could expect that if a metallic NP, when illuminated with a given optical frequency (*i.e.* color) and from a certain direction, generates a strong (weak) localized field in one point, then a local source of the same frequency placed at that point will emit efficiently (badly) in that direction. This is a fundamental concept relevant to all applications of metallic NPs to manipulate light.



 

### Surface enhanced Raman scattering

In surface enhanced Raman scattering (SERS), extraordinarily strong Raman scattering signals are detected from molecules in the vicinity of NPs and NP clusters that are illuminated at their plasmon resonance frequency. A number of reviews and textbooks exist on SERS. While for molecules in very close proximity to the metal surface, direct electron transfer may increase the Raman polarizability,[99] the main contribution to the SERS signals arises from the strongly enhanced local electric fields of plasmonic NPs.[100] The Raman signal is proportional to the product of the local electric field intensities at the incident frequency $|\boldsymbol{E}(\omega)|^2$ and at the Stokes shifted frequency $|\boldsymbol{E}(\omega')|^2$. Since the Stokes shift is usually small in comparison to the LSPR width, it is usually taken as a reasonable approximation that the Raman enhancement is proportional to the fourth power of the local field at the incident frequency $|\boldsymbol{E}(\omega)|^4$.[100] Current knowledge on SERS goes beyond this approximation and quantitative calculations are possible.[101] Metallic NPs, in particular silver, gold and copper, are the preferred substrates for SERS. The strongest SERS enhancement occurs under conditions where the incident and Raman scattered photons are both strongly enhanced, *i.e.* the LSPRs of the NPs are tuned to include both incident and scattered wavelengths. For that, it should be taken into account that the presence of adsorbed molecules will shift the LSPR spectral position.[100] The local fields may be so strongly enhanced that Raman signals from single molecules may be observed.[102–108] The principles of SERS are meanwhile well understood,[109] and current efforts are focused on developing new shapes as well as ordered arrays of metallic NPs to obtain more efficient and controlled SERS.[110–115]

### Fluorescence excitation and emission

The rate of fluorescence photons emitted by a fluorophore is given by:

$$I_F = \Gamma_{exc}\frac{\Gamma_r}{\Gamma_r + \Gamma_{nr}} = \Gamma_{exc}QE \quad (7)$$

where $\Gamma_{exc}$ is the excitation rate, $\Gamma_r$ is the radiative and $\Gamma_{nr}$ the non-radiative de-excitation rates, and QE the fluorescence quantum efficiency. Metallic NPs near a fluorophore may influence all the rates involved in fluorescence.[92,116–123] Depending on its relative position and orientation with respect to the NPs, a fluorophore may experience an enhanced or suppressed electric field, leading to a higher or lower excitation rate, respectively, in comparison to a fluorophore in free space.

The de-excitation rates (*i.e.* the fluorescence lifetime) may be influenced too. In very close proximity to the metal surface, typically closer than 15 nm, direct energy transfer to the metal prevails, which leads to dominant increase of the non-radiative decay rate and the fluorescence emission is strongly suppressed. For larger separation distances, and up to roughly one wavelength, the radiative rate is influenced by variations in the local photonic mode density (PMD). If a fluorophore is placed in a region of high (low) photonic mode density at the emission frequency, the probability of photon emission and thus the radiative decay rate is higher (lower).[117,123] The photonic mode density depends on the orientation of the emission transition dipole of the fluorophore, *e.g.* for a given separation distance from a gold nanosphere, a fluorophore oriented parallel to the NP surface may experience a low PMD whereas a fluorophore perpendicular to the surface may experience a high PMD. All the aforementioned effects are proportional to the spectral overlap between the absorption of the metal NP and the fluorescence emission.

Though it is quite demanding to obtain absolute values for the PMD, variations of the PMD relative to a reference situation are relatively easy to obtain by electric field calculations. Based on reciprocity, the PMD at a given point is proportional to the result of the coherent superposition of fields generated by plane waves incident from all possible directions ($4\pi$ solid angle). For example, in order to obtain the relative PMD for a fluorophore in a given position relative to a NP system, what one needs to do is to calculate the electric field at the fluorophore position, along the dipole orientation, produced by far field plane waves incident from all possible directions, and compare it to the field produced on a reference homogeneous medium (*e.g.* vacuum).

One should note that regions of high excitation field and high PMD may not coincide. First, fluorescence excitation usually takes place from one direction (*e.g.* a laser beam) or a small set of directions (*e.g.* a lens with a limited numerical aperture). The near field distribution obtained when a system is illuminated from a given direction is, in general, different from the one obtained when illumination occurs from all directions. Second, the Stokes shift of fluorescence is not negligible in comparison to the typical widths of plasmon resonances (as is the case in Raman scattering). The response of a NP or a set of NPs at the excitation and emission frequencies may be largely different. And finally, the transition dipoles for absorption and emission of a fluorophore may not have identical orientations.

In summary, the fluorescence emission of a fluorophore near metallic NPs may be suppressed (quenched) or enhanced:

**Quenching.** A suppression of the fluorescence emission in comparison to the free space situation could be due to a dominant reduction of $\Gamma_{exc}$, of QE, or both. The near field distribution around a resonant NP or NP system may present regions where the field component along the absorption dipole of a fluorophore is suppressed, leading to a reduced $\Gamma_{exc}$. For fluorophores with a high intrinsic QE, the presence of the NPs may lead to a decrease of the QE due to a reduced $\Gamma_r$ product of a low PMD. At short separation distances, typically below 15 nm, direct energy transfer to the metal contributes in a dominant way to $\Gamma_{nr}$ leading to a strong quenching.

**Enhancement.** An increase of the fluorescence emission in comparison to the free space situation may be due to a dominant increase of $\Gamma_{exc}$, or of QE, or both. The near field distribution around a resonant NP or NP system may present regions where the field component along the absorption dipole of a fluorophore is enhanced, leading to an increased $\Gamma_{exc}$. For fluorophores with a low intrinsic QE, the presence of the NPs may lead to an increase of QE due to an enhanced $\Gamma_r$ product of a high PMD.[124] If the excitation is high enough to saturate the fluorescence emission, a fluorescence enhancement due to an increased $\Gamma_r$ may be visible also for fluorophores with intrinsic QE close to 1.

Quantifying fluorescence quenching and enhancement is not a trivial task because there are several processes taking place simultaneously. In particular in ensemble measurements, the overall signal obtained comes from fluorophores with different positions and orientations relative to the plasmonic structure. Furthermore, when a fluorophore couples efficiently to a plasmonic structure, the angular patterns of excitation and emission may be strongly modified[12,125] and therefore, a quantitative assessment of the excitation directions as well as the collection angles is necessary.[93] More about directionality is discussed in the next paragraphs. One more aspect, common to most fluorophores that has been left out, is that excited molecules may undergo inter-system crossing to triplet states. Nearby plasmonic structures can also influence the triplet state de-excitation.[123] For these reasons, experiments involving single NPs and single fluorophores have provided the most detailed and quantitative information.[93,116,121,124,125]

### Optical antennas

An antenna, as is the case of traditional microwave and radio-frequency antennas, is a mediator between far-field radiation and local fields (currents) in an electronic circuit. In analogy, due to their strong interaction with light, single as well as arrays of metallic NPs have been investigated as optical antennas.[12,125–127]

As discussed in previous sections, metallic NPs are able to efficiently collect far field radiation and focus it into local fields (near fields) confined to regions of space with dimensions well below the size of a wavelength, *i.e.* metallic NPs are efficient optical *receivers*. As optical *emitters* metallic NPs may enhance decay rates of a local source, for example, a fluorophore. When the resonance of a metallic NP or NP array is properly tuned, it can convert a relatively bad fluorophore into a super-emitter. The radiative rate $\Gamma_r$ becomes so fast that overtakes any other non-radiative processes and boosts the quantum efficiency to near unity. This effect is called super-emission and presents a decay in the picosecond timescale. Bright molecule emission with a lifetime of ~20 ps was recently observed for the first time in the gap of a bow-tie optical antenna,[124] *i.e.* two triangular-prism shaped NPs plasmonically coupled. In addition, an optical antenna may influence the spectral response of an emitter as well. An emitter coupled to an optical antenna will emit more efficiently at the frequencies for which the antenna is resonant.[128] This can be understood as the spectral distribution of the photonic mode density.

Another important feature of an antenna is its directionality. An optical antenna may receive or emit light from different directions with unlike efficiencies. Recent calculations and experiments on individual arrays of NPs[91,93,95,97,125,129] have enabled the investigation of directionality on optical antennas, independently from the other influences of the antenna. Several optical antenna designs have been demonstrated to direct photon emission efficiently.[91,93,97,125,130] Directionality needs to be taken into account in every experiment involving optical antennas because it may strongly affect the experimental excitation and collection efficiencies.[93] Properly designed and fabricated optical antennas hold potential to offer unique high quantum efficiency super-bright single-photon sources with strong directionality for diverse applications.

### Sensing surface reactions

Metallic NPs have been used in sensing for a while now. Typically, the NP surface is modified with molecules containing a recognition site for the target analyte. The interaction between the modified NP and the analyte may be detected in various ways. Probably the most prominent examples are "sandwich" stripe tests, *e.g.* like pregnancy tests, where gold NPs containing specific antibodies on their surface first bind to a target protein or enzyme, which in turn binds to other specific antibodies fixed on a particular area of the stripe, immobilizing the NPs and thereby indicating the reaction. In these kinds of positive/negative biosensors, the LSPR of gold NPs provide the visible color needed to identify that the reaction took place.

An alternative label-free biosensing scheme, which can provide quantitative information about the presence of an analyte, is based on the fact that the spectral position of the LSPR modes depends on the dielectric properties of the immediate environment of the NP. Binding of the analyte on the NP surface modifies the dielectric environment and therefore the LSPR shifts spectrally. Typically target molecules have a higher refractive index than the supporting buffer and the LSPR shifts to the red. For identical refractive changes, LSPRs at longer wavelengths present a larger shift.[74,131–133] This effect has been exploited to realize a number of label-free biosensors based on bulk NP colloids as well as on individual NPs.[72,77,131,133–138] Other kinds of sensors have been developed based on the plasmonic properties of metallic NPs. Examples include sandwich biosensors based on fluorescence quenching[139] or SERS.[114,140,141]

### Non-linear nano-optics

Metallic NPs provide many opportunities for novel non-linear nanoscale photonic devices. First, the strong localized LSPR fields may be used to excite multi-photon and non-linear processes in the vicinity of metallic NPs. Second, metals themselves have a particularly strong non-linear behavior in comparison to dielectrics. For example, the third-order nonlinear susceptibility of gold is more than three orders of magnitude larger than the susceptibility of nonlinear crystals such as KDP, KTP or LiNbO3.[142] Research in non-linear effects and applications with metallic NPs is just beginning. Some illustrative examples are the two-photon luminescence used to characterize metallic NPs and arrays,[127,143] control of the non-linear frequency conversion intensity by tuning the gap between two gold NPs[144,145] and the detection of small NPs by third harmonic generation.[146] The use of optical antennas in non-linear optical nanodevices has been proposed,[147] although the design and fabrication is a considerable challenge because, in addition to the current difficulties in fabricating accurate nanoscale devices, here different optical wavelengths are involved.

## 7 Manipulation of heat at the nanoscale

Metallic NPs are very inefficient fluorophores with fluorescence quantum yields of about $10^{-5}$ or less. As a result, almost all light absorbed by the NPs is transformed into heat. Due to the enhanced absorption, illumination of metal NPs at their LSPR frequencies leads to significant heat generation by the NPs.[87,148–150]

 

### Heat generation

Heat generation after LSPR excitation arises from fast dephasing of the coherent electronic motion in conjunction with rapid energy transfer to the metal crystal lattice.[81,151,152] This heat generation mechanism is extremely fast and thermalization occurs in a time of the order of several picoseconds. That means that for most practical applications, the NPs become hot immediately upon illumination. On the other hand, the temperature increase of the surrounding medium will take a longer time that is determined by heat conduction (*i.e.* by the heat capacity and thermal conductivity of the medium). Experimental determination of heat dissipation and the temperature field around NPs is not a simple task, in particular for small NPs and when only small regions are heated.[148,153] Nevertheless, the heat diffusion equation can be solved numerically or analytically and accurate results are obtained because all parameters involved are known precisely. For example, we take a spherical NP in a homogeneous medium, for which the time dependent solution of the heat equation is known.[154] The stationary solution (*i.e.* for $t \rightarrow \infty$) for the temperature increase of the surrounding medium as a function of the distance $r$ to the NP is given by a simple formula:

$$\Delta T(r) = \frac{I\sigma_{abs}}{4\pi\kappa r} \qquad r>R \qquad (8)$$

where $I$ is the light power density illuminating the NP, $R$ and $\sigma_{abs}$ are the NP radius and absorption cross-section, respectively, and $\kappa$ the thermal conductivity of the surrounding medium. The time $\tau$ necessary to reach half the maximum (steady state) temperature at the NP surface can be estimated as $\tau = R^2/\alpha$,[155] where $\alpha$ is the thermal diffusivity of the surrounding medium.

As an example, Fig. 12 shows the spatial and temporal dependence of the temperature increase $\Delta T$ for the case of a gold NP with $R = 40$ nm, in water, illuminated at its LSPR with three different moderate power densities. This example emphasises the two main features of optical heating by metallic NPs: (i) it is highly confined spatially to the close vicinity of the NP. The temperature increase is limited to small regions with typical length scales of some tens to hundreds of nanometres. In very small regions the thermal response of materials may not be the same as in bulk. For example, a metallic NP in water may have surface temperatures well above 100 °C without boiling. And (ii) heating is extremely fast. Half the maximum temperature is reached in less than 50 ns! This can be considered as an instantaneous temperature jump for most practical applications.

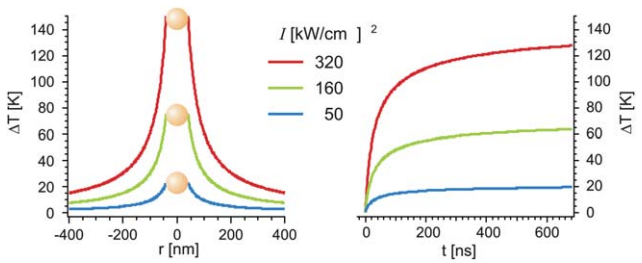


**Fig. 12** Photothermal heating of water by a gold NP. Temperature increase $\Delta T$ of water as functions of the distance $r$ and time $t$ due to heat generation by a gold NP with a diameter of 80 nm, illuminated at its plasmon resonance (532 nm) with three different power densities, which correspond to a laser intensity of 10, 5, and 1.4 mW focused on a spot of 1 mm.

### NPs as optically controlled nanoscopic sources of heat

Metallic NPs may be exploited as versatile, remotely controlled nanoscopic sources of heat. They can be switched on and off, very rapidly (*i.e.* in just a few ns) simply by switching on and off a laser. The rate of absorption is determined by the absorption cross-section and the laser intensity for CW laser, or the pulse width and energy for pulsed lasers. Depending on the relative balance of the rate of absorption and the rate of cooling, various regimes can be identified:

**Photothermal heating.** At low rates of excitation the NPs are able to dissipate the generated heat leading to an increase of the temperature in the surrounding medium.

**Bubble formation.** Short laser pulses (fs to ns) of relatively high energies may lead to bubble formation around the NP.[156,157]

**Melting and surface ejection.** At higher absorption rates, *e.g.* obtained with higher pulse energy ns or fs lasers, the NP accumulates important amounts of heat and may melt.[158] If the NPs are supported on a surface, the melted NPs may be ejected from the substrate. If femtosecond pulses are used, ablation leads to pressure build-up underneath the NPs leading to a high-speed ejection without melting, *i.e.* preserving the NP shape.[159]

**Coherent lattice oscillations.** Femtosecond pulses of low intensity induce coherent oscillation of the NP crystal lattice.[160] These oscillations can have a frequency, which depends on the NP size, shape, and interparticle distance.[160–162]

Applications of metallic NPs as nanoscopic, optically controlled sources of heat are being explored taking advantage of these different regimes. Below we discuss some of the most prominent examples upto today.

### Controlled release

The ability of NPs to produce important amounts of heat locally, triggered by laser illumination, has been exploited in different schemes of controlled release.[163] Controlled release from loaded liposomes decorated with metallic NPs has been achieved by controlled temperature increase[164] using CW illumination or light bursts,[165] as well as by generation of nano-bubbles that disrupt liposome using sub-ns pulses.[166] Another successful strategy is the use of thermoresponsive polymer shells as carriers; the heat produced by the NPs leads to swelling of the polymer and subsequent release.[167,168] Laser triggered release was achieved from layer-by-layer polyelectrolyte shells which could be ruptured by NP heating.[169–171]

Controlled release of single stranded DNA has been demonstrated too, using gold NP functionalized with double stranded DNA which dehybridizes upon NP heating, releasing single stranded DNA for gene therapy.[172,173] This approach could be extended to messenger RNA therapies. New schemes for

controlled release are continuously being reported using increasingly complex systems and NPs, such as gold nano cages.[44]

### Cancer therapy

If attached to the membrane of a biological cell, the heat produced by a NP can disrupt the membrane and lead to cellular death. If the NPs are selectively attached to diseased cells, then photothermal heating of NPs becomes a therapeutic method,[73] which has proven capable of destroying cancerous cells both *in vitro* and *in vivo*.[47,174,175] In particular, gold nanorods and nanoshells are used for this purpose because they can be heated efficiently with wavelengths in the "biological window" of the NIR.[176,177] Current efforts are focused on expanding this methodology by conjugating the NPs with antibodies in order to optimise specific binding to cancerous cells.

### Nanoscale thermodynamics

Current optical microscopy methods provide superb detail of nanoscopic systems with superresolution.[178] Structures and pathways can be determined with great precision. Still, full understanding of the functionality of a system requires additional energetic information. This kind of information has been traditionally obtained by bulk techniques such as differential scanning calorimetry. Metallic NPs offer a totally new opportunity: local thermal manipulation and thermodynamics experiments on the nanoscale! Research on this field is only starting[179,180] now that optical heating of NPs is well understood. Metallic NPs provide the fundamental element: the nanoscopic source of heat. The challenge remains to design each experiment suitably to extract the desired information from each particular system. For example, by analyzing the 2D Brownian motion performed by optically heated gold NPs over a phospholipid membrane, it was possible to measure locally the gel–fluid phase transition temperature and phase transition front velocity of various phospholipid membranes.[180]

### Catalysis and materials processing

Naturally, optical heating of metallic NPs can be used anywhere where local or remotely controlled heating could be advantageous. Nanoscale processing of polymers has been demonstrated using an optically trapped and heated metallic NP,[181] and NPs have been embossed into polymer films too.[182] Another barely unexplored area where metallic NPs hold great potential is local, temperature driven catalysis.[183]

## 8 Manipulation of forces at the nanoscale

Optical forces have been well studied both theoretically and experimentally for various applications such as optical trapping and manipulation of small particles and even biological cells. Here we make a basic introduction and discuss the particular issues related to metallic NPs. In particular, we discuss how optical fields exert forces on metallic NPs, and how the near fields of LSPRs can be used for optical manipulation.

### The Maxwell stress-tensor

Forces in electromagnetic fields arise from the conservation of linear momentum. We will not make a derivation here, but this conservation law is a consequence of Maxwell's equations and the Lorenz force law. For electromagnetic waves the momentum density in a medium with dielectric constant $\varepsilon$ and magnetic susceptibility $\mu$ is given by the Maxwell stress tensor:

$$\overleftrightarrow{\boldsymbol{T}}(\boldsymbol{r},t)=\left[\varepsilon\varepsilon_0\boldsymbol{EE}-\mu\mu_0\boldsymbol{HH}-\left(\frac{1}{2}\varepsilon\varepsilon_0E^2+\mu\mu_0H^2\right)\overleftrightarrow{\boldsymbol{I}}\right] \quad (9)$$

where $\overleftrightarrow{\boldsymbol{I}}$ is the unit dyadic. This stress tensor gives the flux of momentum across an area and is the starting point for all field-based optical force calculations. The average mechanical force acting on an arbitrary body within the close surface $V$ is obtained by integrating the momentum flux over the surface:

$$\langle\boldsymbol{F}\rangle=\int_V\overleftrightarrow{\boldsymbol{T}}(\boldsymbol{r},t)\boldsymbol{n}(\boldsymbol{r})\mathrm{d}a \quad (10)$$

The force is completely determined by the electric and magnetic fields on the surface $V$, therefore the whole information is contained in the electromagnetic field. Furthermore, as the enclosing surface is arbitrary the same results are obtained if the fields are computed at the surface of the body or in the far field. Here it is important to note that the fields used to calculate the force are the self-consistent fields of the problem, *i.e.* the superposition of the incident and scattered fields. The described Maxwell's stress tensor method is a versatile tool and can be applied *via* numerical methods in a variety of different scenarios ranging from NPs in an evanescent field[184,185] to arrays of NPs[186,187] in focused beams just to mention a few examples.

Besides energy and momentum, an electromagnetic field can also carry angular momentum which exerts a mechanical torque on an irradiated structure. This torque can also be calculated from the conservation law for angular momentum; the expression of the time averaged torque for a monochromatic field can be represented as:

$$\langle\boldsymbol{N}\rangle=\int_V\langle\overleftrightarrow{\boldsymbol{T}}(\boldsymbol{r},t)\times\boldsymbol{r}\rangle\boldsymbol{n}(\boldsymbol{r})\mathrm{d}a \quad (11)$$

### The Rayleigh regime

When the diameter of the particle is significantly smaller than the wavelength of light, the particle can be treated as a small dipole $\boldsymbol{p}$. Under this approximation, the total force acting on the particle is:

$$\boldsymbol{F}=(\boldsymbol{p}\nabla)\boldsymbol{E}+\dot{\boldsymbol{p}}\times\boldsymbol{B}+\ddot{\boldsymbol{r}}\times(\boldsymbol{p}\nabla)\boldsymbol{B} \quad (12)$$

The force consists of three terms. The first one originates from the inhomogeneous electric field, the second is the Lorentz force, and the third is due to the motion in the inhomogeneous magnetic field. The third term usually is negligible compared to the other two. Note that in this dipole approximation the fields appearing in eqn (12) are the exciting fields, propagating or evanescent; it is assumed that the small dipole does not alter the fields. Because this situation is less rigorous than the general formalism based on the Maxwell's stress tensor where the



 

self-consistent fields are taken into account, one cannot expect quantitative results, especially for resonant metallic NPs which have a strong dipole moment. Still, its simplicity makes the Rayleigh approximation very useful for a first estimate and to understand phenomena and experimental situations qualitatively. Within this approximation the force averaged over one cycle is given by:

$$\langle \boldsymbol{F} \rangle = \frac{\alpha'}{2} \nabla \left\langle |\boldsymbol{E}|^2 \right\rangle + \omega \frac{\alpha''}{2} \langle \boldsymbol{E} \times \boldsymbol{B} \rangle \qquad (13)$$

where $\omega$ is the frequency of the optical field and $\alpha = \alpha' + i\alpha''$ is the NP polarizability. The first term of eqn (13) is denoted as the *gradient force* and is caused by the field inhomogeneities. A positive gradient force points towards regions of high field intensity. The second term, called the *scattering force*, is a consequence of momentum transfer from the radiation field to the particle. The scattering force receives this name because usually, non-absorbing particles are used in optical traps. But in fact, this force may be decomposed into scattering and absorption components:[188]

$$\omega \frac{\alpha''}{2} \langle \boldsymbol{E} \times \boldsymbol{B} \rangle = \boldsymbol{F}_{\mathrm{sca}} + \boldsymbol{F}_{\mathrm{abs}} = \frac{n}{c} \langle \boldsymbol{S} \rangle \sigma_{\mathrm{sca}} + \frac{n}{c} \langle \boldsymbol{S} \rangle \sigma_{\mathrm{abs}} \qquad (14)$$

here $n$ is the medium refractive index, $c$ the speed of light and $\boldsymbol{S}$ the Poynting vector. Therefore, this term is called the *scattering-plus-absorption force* and points in the direction of the field propagation.

## Optical forces on metallic NPs

For a given field distribution, the optical forces acting on a particle depend on its polarizability. In order to illustrate the possible situations, Fig. 13 shows the spectral dependence of $\alpha'$ and $\alpha''$ for spherical NPs made of Ag and Au.

First, $\alpha''$ takes a maximum value at the LSPR wavelength, which corresponds to enhanced absorption and scattering cross-sections and thus stronger scattering-plus-absorption forces.[190] Depending on the size of the NP, these forces may be dominated by scattering or absorption processes. For example, in the case of silver, $\alpha''$ is about 100 times larger at the $\lambda_{\mathrm{LSPR}} \approx 350$ nm than at 500 nm, which leads to a scattering-plus-absorption force about 70 times stronger. Gold presents a similar but less dramatic behavior due to larger losses; in addition $\alpha''$ of gold remains relatively large at wavelengths below the LSPR due to strong interband transitions.

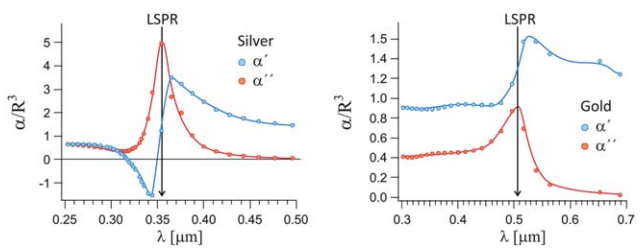


**Fig. 13** Quasistatic polarizability of (A) silver and (B) gold spherical NPs, calculated from eqn (1) and dielectric constants from ref. 189.

Second, $\alpha'$ presents large variations near the plasmon resonance. For metals with low losses (*e.g.* Ag, Al) $\alpha'$ takes negative values for wavelengths below the LSPR, crosses zero near the LSPR and becomes positive for longer wavelengths. Then, depending on the detuning of the laser wavelength with respect to the LSPR, the gradient force may be attractive (towards regions of high field intensity), null, or repulsive.[190]

## Manipulating metallic NPs with laser beams

If a particle for a given wavelength has a positive $\alpha'$, the gradient force will cause the particle to move towards regions of maximum field intensity. This is the basis of optical trapping of dielectric particles in tightly focused laser beams. The scattering force, on the other hand, will push the particle in the propagation direction. Thus the usual condition for optical trapping of dielectric (non-resonant) particles in a single beam is that the gradient force in the longitudinal direction surpasses the scattering force.

Let us first analyze the case of metallic NPs with low losses such as Ag or Al. Close to the LSPR, it is impossible to trap a NP with a single laser beam because the gradient force becomes almost zero and the scattering-plus-absorption force becomes maximum. If the laser is detuned toward shorter wavelengths, $\alpha'$ becomes negative and the gradient force repulsive! Doughnut-shaped Laguerre–Gaussian beams, which have a minimum intensity in the center, have been used to trap atoms near resonant absorption. These so-called "dark traps" or "blue detuned traps" have the advantage that minimize the interaction of the trapped object with the laser (*e.g.* a metallic NP would be less heated) but have, to our knowledge, not yet been implemented for metallic NPs. Controlled detuning to wavelengths above the LSPR can be very advantageous for NP trapping in focused beams because $\alpha''$ drops rapidly and $\alpha'$ remains positive and relatively large. This is a common behavior for NPs with low or high losses. In these regions metallic NPs can be tweezed optically much more efficiently than dielectric particles.[188,191–195] Tweezing dielectric particles much smaller than a micrometre becomes impractical because of the high laser intensities needed and the difficulties in detecting those particles optically. In contrast, due to their large polarizability, gold NPs as small as 18 nm have been readily tweezed using moderate laser powers and a single focused Gaussian beam.[194]

Metallic NPs with high losses such as Au have a positive $\alpha'$ for all wavelengths across the LSPR but the very large scattering plus absorption force makes it impractical to trap Au NPs with a single Gaussian laser beam near the LSPR. The NP is pulled toward the center of the beam by the positive gradient force but also pushed strongly in the beam propagation direction. This particular combination of forces has been exploited to print single gold NPs on surfaces with spatial resolution of a few tens of nanometres.[69] In order to trap gold NPs near their LSPR two counter-propagating beams would be necessary, in order to cancel the scattering plus absorption force out, or to use radially polarized vortex beams that make use of the scattering forces to trap NPs in a minimum of intensity.[196,197]

### Optical trapping using the LSPR near field

Due to their strong spatial confinement, evanescent near fields may generate considerable gradient forces and thus be used for optical manipulation.[185] Pioneering work in these directions involved surface bound evanescent fields in total internal reflection configurations.[198,199] One can use evanescent fields scattered by sub-wavelength objects in order to achieve 3D optical field confinement beyond the diffraction limit with the potential to trap Rayleigh objects.[16,185,200] LSPR fields supported at the surface of metallic NPs and nanostructures offer new opportunities in optical manipulation: (i) the enhancements of LSPR fields are expected to decrease the trapping laser intensity requirements, and (ii) the ability of LSPR fields to be confined down to the sub-wavelength regime opens new perspectives to scale optical trapping down to the nanometre scale. In particular, light confinement at the extremity of a metallic tip[201,202] or at the output of a hole in a metallic film[203,204] was predicted to enable optical trapping of very small objects down to a few tens of nanometres. Optical trapping using a variety of plasmonic structures has been demonstrated in recent years,[205–207] including a plasmonic dipole antenna formed by a pair of metal nanorods spaced by a nanometric gap which enabled the efficient trapping of 10 nm gold NPs.[208]

## 9 Concluding remarks

We have described the basic physics of LSPRs and the most relevant theoretical and numerical methods for their calculation. By means of examples we have explained the main features of LSPRs and widely used methods for the optical detection of metallic NPs. Finally, mentioning some prominent experimental and technological applications of metallic NPs we have portrayed how they can be used for the nanoscale manipulation of light, heat and forces.

It is important to note that all the phenomena described in this article, which have been classified in light, heat and force effects, do actually take place simultaneously when a metallic NP is illuminated. This combination of effects must always be kept in mind when dealing with resonant metallic NPs. It may as well lead to experimental complications or advantages. For example, when a NP is optically trapped in a highly intense field, a considerable amount of heat is produced. This could be a disadvantage for trapping because of the incremented Brownian motion, or could be exploited for contact-less thermal processing of materials.[181]

Other interesting examples where the combination of effects is cleverly exploited include near field scanning optical microscopy using as probe an optically trapped metallic NP.[195] This contact-free near field microscope probe may then be utilized for fluorescence or near field imaging. Another possibility is to trap optically metallic NPs, using dark-field microscopy for position feedback, in order to investigate single NP properties without the influence of a nearby interface[209] or to create *in situ* hot-spots for SERS.[210] One more example is the recent demonstration of a novel optical trapping method exploiting the non-linear polarizability of gold NPs.[211] The investigation of the interaction of metallic NPs with light is currently at its maximum activity, and will certainly continue to reveal novel phenomena and applications.

## Acknowledgements

FDS thanks Maurizio Righini for fruitful discussions, and CONICET, UBA and ANPCyT for financial support. EAC thanks SECYT UNC and CONICET for financial support.

## References

1 A. Sommerfeld, *Electrodynamics*, Academic Press, New York, 1952.
2 R. W. Wood, *Philos. Mag.*, 1902, **4**, 396–402.
3 J. C. M. Garnett, *Philos. Trans. R. Soc. London, Ser. A*, 1904, **203**, 385–420.
4 G. Mie and G. Beirträge, *Ann. Phys.*, 1908, **25**, 37.
5 E. Kretschmann and H. Reather, *Z. Naturforsch., A: Astrophys., Phys. Phys. Chem.*, 1968, **23**, 2135–2136.
6 A. Otto, *Z. Phys.*, 1968, **216**, 398–410.
7 M. Fleischmann, P. J. Hendra and A. J. McQuillan, *Chem. Phys. Lett.*, 1974, **26**, 163–166.
8 D. L. Jeanmarie and R. P. van Duyne, *J. Electroanal. Chem.*, 1977, **84**, 1–20.
9 H. Raether, *Surface Plasmons on Smooth and Rough Surfaces and on Gratings*, Springer Verlag, 1988.
10 W. Knoll, *Annu. Rev. Phys. Chem.*, 1998, **49**, 569–638.
11 H. Ditlbacher, A. Hohenau, D. Wagner, U. Kreibig, M. Rogers, F. Hofer, F. R. Aussenegg and J. R. Krenn, *Phys. Rev. Lett.*, 2005, 257403.
12 T. H. Taminiau, F. D. Stefani and N. F. van Hulst, *Nano Lett.*, 2011, **11**, 1020–1024.
13 F. Hao, C. L. Nehl, J. H. Hafner and P. Nordlander, *Nano Lett.*, 2007, **7**, 729–732.
14 S. Asano and G. Yamamoto, *Appl. Opt.*, 1975, **14**, 29–49.
15 H. Xu, *Phys. Lett. A*, 2003, **312**, 411–419.
16 L. Novotny and B. Hecht, *Principles of Nano-optics*, Cambridge University Press, 2006.
17 B. T. Draine and J. Goodman, *Astrophys. J.*, 1993, **405**, 685–697.
18 B. T. Draine and P. J. Flatau, *J. Opt. Soc. Am. A*, 1994, **11**, 1491.
19 Y. Xiong, J. M. Mclellan, J. Chen, Y. Yin, Z.-y. Li and Y. Xia, *J. Am. Chem. Soc.*, 2005, **127**, 17118–17127.
20 M. A. Mahmoud, B. Snyder and M. A. El-Sayed, *J. Phys. Chem. C*, 2010, **114**, 7436–7443.
21 T. R. Jensen, G. C. Schatz and R. P. Van Duyne, *J. Phys. Chem. B*, 1999, **103**, 2394–2401.
22 A. J. Logsdail, N. J. Cookson, S. L. Horswell, Z. W. Wang, Z. Y. Li and R. L. Johnston, *J. Phys. Chem. C*, 2010, **114**, 21247–21251.
23 J. Zhao, A. O. Pinchuk, J. M. Mcmahon, S. Li, L. K. Ausman, A. L. Atkinson and G. C. Schatz, *Acc. Chem. Res.*, 2008, **41**, 1710–1720.
24 E. K. Payne, K. L. Shuford, S. Park, G. C. Schatz and C. A. Mirkin, *J. Phys. Chem. B*, 2006, **110**, 2150–2154.
25 K. L. Kelly, E. Coronado, L. L. Zhao and G. C. Schatz, *J. Phys. Chem. B*, 2003, **107**, 668–677.
26 M. Yurkin and A. Hoekstra, *J. Quant. Spectrosc. Radiat. Transfer*, 2007, **106**, 558–589.
27 P. Chaumet, A. Rahmani and G. Bryant, *Phys. Rev. B: Condens. Matter*, 2003, **67**, 165404.
28 R. Schmehl, B. M. Nebeker and E. D. Hirleman, *J. Opt. Soc. Am. A*, 1997, 3026–3036.
29 A. Penttila, E. Zubko, K. Lumme, K. Muinonen, M. Yurkin, B. Draine, J. Rahola, A. Hoekstra and Y. Shkuratov, *J. Quant. Spectrosc. Radiat. Transfer*, 2007, **106**, 417–436.
30 E. Zubko, D. Petrov, Y. Grynko, Y. Shkuratov, H. Okamoto, K. Muinonen, T. Nousiainen, H. Kimura, T. Yamamoto and G. Videen, *Appl. Opt.*, 2010, **49**, 1267–1279.
31 E. M. Perassi, L. R. Canali and E. A. Coronado, *J. Phys. Chem. C*, 2009, **113**, 6315–6319.
32 A. Taflove, *Computational Electrodynamics*, Artech House, Boston, 1995.
33 J. P. Kottmann and O. J. F. Martin, *IEEE Trans. Antennas Propag.*, 2000, **48**, 1719–1726.
34 K. S. Yee, *IEEE Trans. Antennas Propag.*, 1966, **14**, 302–307.

 

35 A. Taflove, *IEEE Trans. Electromagn. Compat.*, 1980, **22**, 191–202.
36 A. Taflove and S. C. Hagness, *Computational Electrodynamics: The Finite-Difference-Time-Domain-Method*, Artech House, 3rd edn, 2005.
37 E. R. Encina and E. A. Coronado, *J. Phys. Chem. C*, 2007, **111**, 16796–16801.
38 A. L. Schmucker, N. Harris, M. J. Banholzer, M. G. Blaber, K. D. Osberg, G. C. Schatz and C. A. Mirkin, *ACS Nano*, 2010, **4**, 5453–5463.
39 J. Dorfmüller, R. Vogelgesang, W. Khunsin, C. Rockstuhl, C. Etrich and K. Kern, *Nano Lett.*, 2010, **10**, 3596–3603.
40 S.-D. Liu and M.-T. Cheng, *J. Appl. Phys.*, 2010, **108**, 034313.
41 J. Krenn, G. Schider and W. Rechberger, *Appl. Phys.*, 2000, **77**, 3379–3381.
42 S. Barbosa, A. Agrawal, L. Rodríguez-Lorenzo, I. Pastoriza-Santos, R. a. Alvarez-Puebla, A. Kornowski, H. Weller and L. M. Liz-Marzán, *Langmuir*, 2010, **26**, 14943–14950.
43 C. Hrelescu, T. K. Sau, A. L. Rogach, F. Jäckel, G. Laurent, L. Douillard and F. Charra, *Nano Lett.*, 2011, **11**, 402–407.
44 M. S. Yavuz, Y. Cheng, J. Chen, C. M. Cobley, Q. Zhang, M. Rycenga, J. Xie, C. Kim, K. H. Song, A. G. Schwartz, L. V. Wang and Y. Xia, *Nat. Mater.*, 2009, **8**, 935–939.
45 B. R. Bardhan, W. Chen, C. Perez-torres, M. Bartels, R. M. Huschka, L. L. Zhao, E. Morosan, R. G. Pautler, A. Joshi and N. J. Halas, *Adv. Funct. Mater.*, 2009, **19**, 1–9.
46 J. Yuqiang, N. Nishizawa, H. Kohei, I. Okamoto, H. Ko, M. Shigemoto and R. Shigemoto, *Adv. Mater.*, 2009, **21**, 2309–2313.
47 S. Lal, S. E. Clare and N. J. Halas, *Acc. Chem. Res.*, 2008, **41**, 1842–1851.
48 U. Kreibig, *Optical Properties of Metal Clusters*, Springer, Berlin, 1995.
49 E. Prodan, C. Radloff, N. J. Halas and P. Nordlander, *Science*, 2003, **302**, 419–422.
50 P. Aravind, A. Nitzan and H. Metiu, *Surf. Sci.*, 1981, **110**, 189–204.
51 W. Rechberger, *Opt. Commun.*, 2003, **220**, 137–141.
52 P. Nordlander, C. Oubre, E. Prodan, K. Li and M. I. Stockman, *Nano Lett.*, 2004, **4**, 899–903.
53 M. Schmeits and L. Dambly, *Phys. Rev. B: Condens. Matter*, 1991, **44**, 12706–12712.
54 C. Sönnichsen, B. M. Reinhard, J. Liphardt and A. P. Alivisatos, *Nat. Biotechnol.*, 2005, **23**, 741–745.
55 E. Hao and G. C. Schatz, *J. Chem. Phys.*, 2004, **120**, 357–366.
56 J. P. Kottmann and O. J. F. Martin, *Opt. Lett.*, 2001, **26**, 1096–1098.
57 H. Xu, J. Aizpurua, M. Kall and P. Apell, *Phys. Rev. E: Stat. Phys., Plasmas, Fluids, Relat. Interdiscip. Top.*, 2000, **62**, 4318–4324.
58 K. Li, X. Li, M. I. Stockman and D. J. Bergman, *Phys. Rev. B: Condens. Matter Mater. Phys.*, 2005, **71**, 115409.
59 J. R. Krenn, A. Dereux, J. C. Weeber, E. Bourillot, Y. Lacroute, J. P. Goudonnet, G. Schider, W. Gotschy, A. Leitner, F. R. Aussenegg and C. Girard, *Phys. Rev. Lett.*, 1999, **82**, 2590–2593.
60 B. M. Reinhard, S. Sheikholeslami, A. Mastroianni, A. P. Alivisatos and J. Liphardt, *Proc. Natl. Acad. Sci. U. S. A.*, 2007, **104**, 2667–2672.
61 P. K. Jain and M. A. El-Sayed, *J. Phys. Chem. C*, 2008, **112**, 4954–4960.
62 P. K. Jain and M. A. El-Sayed, *Nano Lett.*, 2007, **7**, 2854–2858.
63 E. R. Encina and E. A. Coronado, *J. Phys. Chem. C*, 2010, **114**, 3918–3923.
64 J. J. Mock, D. R. Smith and S. Schultz, *Nano Lett.*, 2003, **3**, 485–491.
65 J. J. Mock, M. Barbic, D. R. Smith, D. A. Schultz and S. Schultz, *J. Chem. Phys.*, 2002, **116**, 6755.
66 C. Sönnichsen, S. Geier, N. E. Hecker, G. Von Plessen, C. Sönnichsen, J. Feldmann, H. Ditlbacher, B. Lamprecht, J. R. Krenn, F. R. Aussenegg, V. Z.-H. Chan, J. P. Spatz and M. Möller, *Appl. Phys. Lett.*, 2000, **77**, 2949–2951.
67 C. Sönnichsen, T. Franzl, T. Wilk, G. Von Plessen and J. Feldmann, *New J. Phys.*, 2002, **4**, 93.
68 C. Sönnichsen, T. Franzl, J. Feldmann, T. Wilk, O. Wilson and P. Mulvaney, *Phys. Rev. Lett.*, 2002, **88**, 077402.
69 A. S. Urban, A. A. Lutich, F. D. Stefani and J. Feldmann, *Nano Lett.*, 2010, **10**, 4794–4798.
70 S. Schultz, D. R. Smith, J. J. Mock and D. A. Schultz, *Proc. Natl. Acad. Sci. U. S. A.*, 2000, **97**, 996–1001.
71 J. Becker, O. Schubert and C. Sönnichsen, *Nano Lett.*, 2007, **7**, 1664–1669.
72 G. Raschke, S. Kowarik, T. Franzl, C. Sönnichsen, T. A. Klar, A. Nichtl, K. Kürzunger and J. Feldmann, *Nano Lett.*, 2003, **3**, 935–938.
73 X. Huang, P. K. Jain, I. H. El-Sayed and M. A. El-Sayed, *Lasers Med. Sci.*, 2008, **23**, 217–228.
74 G. Raschke, J. Feldmann, S. Brogl, A. S. Susha, A. L. Rogach, T. A. Klar, B. Fieres, N. Petkov, T. Bein, A. Nichtl and K. Kürzinger, *Nano Lett.*, 2004, **4**, 1853–1857.
75 M. Ringler, T. A. Klar, A. Schwemer, A. S. Susha, J. Stehr, G. Raschke, S. Funk, M. Borowski, A. Nichtl, A. Nichtl, K. Kürzinger, K. Ku, R. T. Phillips and J. Feldmann, *Nano Lett.*, 2007, **7**, 2753–2757.
76 K.-H. Su, Q.-H. Wei, X. Zhang, J. J. Mock, D. R. Smith and S. Schultz, *Nano Lett.*, 2003, **3**, 1087–1090.
77 A. D. Mcfarland and R. P. V. Duyne, *Nano Lett.*, 2003, **3**, 1057–1062.
78 K. Lindfors, T. Kalkbrenner, P. Stoller and V. Sandoghdar, *Phys. Rev. Lett.*, 2004, **93**, 037401.
79 V. Jacobsen, P. Stoller, C. Brunner, V. Vogel and V. Sandoghdar, *Opt. Express*, 2006, **14**, 2949–2951.
80 H. Ewers, V. Jacobsen, E. Klotzsch, A. E. Smith, A. Helenius and V. Sandoghdar, *Nano Lett.*, 2007, **7**, 2263–2266.
81 S. Link and M. A. El-Sayed, *Annu. Rev. Phys. Chem.*, 2003, **54**, 331–366.
82 A. Arbouet, D. Christofilos, N. Del Fatti, F. Vallée, J. R. Huntzinger, L. Arnaud, P. Billaud and M. Broyer, *Phys. Rev. Lett.*, 2004, **93**, 127401.
83 S. Berciaud, L. Cognet, G. A. Blab and B. Lounis, *Phys. Rev. Lett.*, 2004, **93**, 257402.
84 L. Cognet, S. Berciaud, D. Lasne and B. Lounis, *Anal. Chem.*, 2008, **80**, 2288–2294.
85 J. P. Wilcoxon, J. E. Martin, F. Parsapour, B. Wiedenman and D. F. Kelley, *J. Chem. Phys.*, 1998, **108**, 9137.
86 E. Dulkeith, T. Niedereichholz, T. Klar, J. Feldmann, G. von Plessen, D. Gittins, K. Mayya and F. Caruso, *Phys. Rev. B: Condens. Matter Mater. Phys.*, 2004, **70**, 1–4.
87 D. Boyer, P. Tamarat, A. Maali, B. Lounis and M. Orrit, *Science*, 2002, **297**, 1160–1163.
88 M. Mansuripur and D. P. Tsai, *Opt. Commun.*, 2011, **284**, 707–714.
89 A. T. Hoop, *Appl. Sci. Res., Sect. B*, 1960, **8**, 135–140.
90 R. J. Potton, *Rep. Prog. Phys.*, 2004, **67**, 717–754.
91 T. H. Taminiau, F. D. Stefani and N. F. van Hulst, *Opt.Express*, 2008, **16**, 10858–10866.
92 F. D. Stefani, K. Vasilev, N. Bocchio, N. Stoyanova and M. Kreiter, *Phys. Rev. Lett.*, 2005, **94**, 023005.
93 T. H. Taminiau, F. D. Stefani and N. F. van Hulst, *New J. Phys.*, 2008, **10**, 105005.
94 R. Carminati, M. Nieto-vesperinas and J.-J. Greffet, *J. Opt. Soc. Am. A*, 1998, **15**, 706–712.
95 A. M. Kern and O. J. F. Martin, *Nano Lett.*, 2011, 0–5.
96 J. A. Schuller, T. Taubner and M. L. Brongersma, *Nat. Photonics*, 2009, **3**, 658–661.
97 T. Pakizeh and M. Käll, *Nano Lett.*, 2009, **9**, 2343–2349.
98 K. Vasilev, W. Knoll and M. Kreiter, *J. Chem. Phys.*, 2004, **120**, 3439–3445.
99 A. Otto, *J. Raman Spectrosc.*, 2005, **36**, 497–509.
100 G. C. Schatz, M. A. Young and R. P. V. Duyne, *Top. Appl. Phys.*, 2006, **103**, 19–46.
101 E. C. Le Ru, J. Grand, N. Félidj, J. Aubard, G. Lévi, A. Hohenau, J. R. Krenn, E. Blackie and P. G. Etchegoin, *J. Phys. Chem. C*, 2008, **112**, 8117–8121.
102 K. Kneipp, H. Kneipp, G. Deinum, I. Itzkan, R. R. Dasari and M. S. Feld, *Appl. Spectrosc.*, 1998, **52**, 175–178.
103 S. Nie and S. R. Emory, *Science*, 1997, **275**, 1102–1106.
104 W. E. Doering and S. Nie, *J. Phys. Chem. B*, 2002, **106**, 311–317.
105 J. Jiang, K. Bosnick, M. Maillard and L. Brus, *J. Phys. Chem. B*, 2003, **107**, 9964–9972.
106 E. Cortés, P. G. Etchegoin, E. C. Le Ru, A. Fainstein, M. E. Vela and R. C. Salvarezza, *J. Am. Chem. Soc.*, 2010, **132**, 18034–18037.
107 H. Xu, E. Bjerneld, M. Käll and L. Börjesson, *Phys. Rev. Lett.*, 1999, **83**, 4357–4360.
108 E. C. LeRu, *J. Phys. Chem. C*, 2007, **111**, 13794–13803.

109 E. C. Le Ru and P. G. Etchegoin, *Principles of Surface-Enhanced Raman Spectroscopy*, Elsevier, Amsterdam, 2009.
110 C. E. Talley, J. B. Jackson, C. Oubre, N. K. Grady, C. W. Hollars, S. M. Lane, T. R. Huser, P. Nordlander and N. J. Halas, *Nano Lett.*, 2005, **5**, 1569–1574.
111 N. Félidj, J. Aubard, G. Lévi, J. R. Krenn, a. Hohenau, G. Schider, a. Leitner and F. R. Aussenegg, *Appl. Phys. Lett.*, 2003, **82**, 3095.
112 H. Wang, C. S. Levin and N. J. Halas, *J. Am. Chem. Soc.*, 2005, **127**, 14992–14993.
113 M. P. Kreuzer, S. Bálint, S. Rao, G. Badenes, P. Miskovský and D. Petrov, *J. Phys. Chem. C*, 2009, **113**, 17724–17729.
114 L. Rodríguez-Lorenzo, R. A. Álvarez-Puebla, I. Pastoriza-Santos, S. Mazzucco, S. Odile, M. Kociak, L. M. Liz-Marzan and F. J. García De Abajo, *J. Am. Chem. Soc.*, 2009, **131**, 4616–4618.
115 J. J. Baumberg, T. A. Kelf, Y. Sugawara, S. Cintra, M. E. Abdelsalam, P. N. Bartlett and A. E. Russell, *Nano Lett.*, 2005, **5**, 2262–2267.
116 P. Anger, P. Bharadwaj and L. Novotny, *Phys. Rev. Lett.*, 2006, **96**, 113002.
117 W. L. Barnes, *J. Mod. Opt.*, 1998, **45**, 661–699.
118 H. Ditlbacher, N. Felidj, J. R. Krenn, B. Lamprecht, A. Leitner and F. R. Aussenegg, *Appl. Phys. B: Lasers Opt.*, 2001, **73**, 373–377.
119 E. Dulkeith, A. C. Morteani, T. Niedereichholz, T. A. Klar, J. Feldmann, S. A. Levi, F. C. J. M. van Veggel, D. N. Reinhoudt, M. Möller and D. I. Gittins, *Phys. Rev. Lett.*, 2002, **89**, 203002.
120 J. Gersten and A. Nitzan, *J. Chem. Phys.*, 1981, **75**, 1139–1152.
121 S. Kühn, U. Håkanson, L. Rogobete and V. Sandoghdar, *Phys. Rev. Lett.*, 2006, **97**, 017402.
122 J. R. Lakowicz, J. Malicka, I. Gryczynski, Z. Gryczynski and C. D. Geddes, *J. Phys. D: Appl. Phys.*, 2003, **36**, 240–249.
123 F. D. Stefani, K. Vasilev, N. Bocchio, F. Gaul, A. Pomozzi and M. Kreiter, *New J. Phys.*, 2007, **9**, 21.
124 A. Kinkhabwala, Z. Yu, S. Fan, Y. Avlasevich, K. Müllen and W. E. Moerner, *Nat. Photonics*, 2009, **3**, 654–657.
125 T. H. Taminiau, F. D. Stefani, N. F. Van Hulst and F. B. Segerink, *Nat. Photonics*, 2008, **2**, 234–237.
126 P. Bharadwaj, B. Deutsch and L. Novotny, *Adv. Opt. Photonics*, 2009, **1**, 438–483.
127 P. Mühlschlegel, H.-J. Eisler, O. J. F. Martin, B. Hecht and D. W. Pohl, *Science*, 2005, **308**, 1607–1609.
128 M. Ringler, A. Schwemer, M. Wunderlich, A. Nichtl, K. Kürzinger, T. Klar and J. Feldmann, *Phys. Rev. Lett.*, 2008, **100**, 203002.
129 A. G. Curto, G. Volpe, T. H. Taminiau, M. P. Kreuzer, R. Quidant and N. F. van Hulst, *Science*, 2010, **329**, 930–933.
130 T. Shegai, V. D. Miljković, K. Bao, H. Xu, P. Nordlander, P. Johansson and M. Käll, *Nano Lett.*, 2011, **11**, 706–711.
131 G. J. Nusz, S. M. Marinakos, A. C. Curry, A. Dahlin, F. Höök, A. Wax and A. Chilkoti, *Anal. Chem.*, 2008, **80**, 984–989.
132 G. J. Nusz, A. C. Curry, S. M. Marinakos, A. Wax and A. Chilkoti, *ACS Nano*, 2009, **3**, 795–806.
133 S. K. Dondapati, T. K. Sau, C. Hrelescu, T. A. Klar, F. D. Stefani and J. Feldmann, *ACS Nano*, 2010, **4**, 6318–6322.
134 P. Englebienne, *Analyst*, 1998, **123**, 1599–1603.
135 N. Nath and A. A. Chilkoti, *Anal. Chem.*, 2002, **74**, 504–509.
136 C. L. Baciu, J. Becker, A. Janshoff and C. Sönnichsen, *Nano Lett.*, 2008, **8**, 1724–1728.
137 K. M. Mayer, S. Lee, H. Liao, B. C. Rostro, A. Fuentes, P. T. Scully, C. L. Nehl and J. H. Hafner, *ACS Nano*, 2008, **2**, 687–692.
138 A. J. Haes, W. P. Hall, L. Chang, W. L. Klein and R. P. Van Duyne, *Nano Lett.*, 2004, **4**, 1029–1034.
139 S. Mayilo, M. A. Kloster, M. Wunderlich, A. Lutich, T. A. Klar, A. Nichtl, K. Ku, F. D. Stefani and J. Feldmann, *Nano Lett.*, 2009, **9**, 4558–4563.
140 C. R. Yonzon, C. L. Haynes, X. Zhang, J. T. Walsh and R. P. V. Duyne, *Anal. Chem.*, 2004, **76**, 78–85.
141 I.-H. Chou, M. Benford, H. T. Beier, G. L. Coté, M. Wang, N. Jing, J. Kameoka and T. A. Good, *Nano Lett.*, 2008, **8**, 1729–1735.
142 J. Renger, R. Quidant, N. van Hulst and L. Novotny, *Phys. Rev. Lett.*, 2010, **104**, 046803.
143 P. Ghenuche, S. Cherukulappurath, T. Taminiau, N. van Hulst and R. Quidant, *Phys. Rev. Lett.*, 2008, **101**, 116805.
144 S. Palomba, M. Danckwerts and L. Novotny, *J. Opt. A: Pure Appl. Opt.*, 2009, **11**, 114030.
145 S. Palomba and L. Novotny, *Phys. Rev. Lett.*, 2008, **101**, 056802.
146 M. Lippitz, M. A. van Dijk and M. Orrit, *Nano Lett.*, 2005, **5**, 799–802.
147 L. Novotny and N. van Hulst, *Nat. Photonics*, 2011, **5**, 83–90.
148 H. H. Richardson, Z. N. Hickman, A. O. Govorov, A. C. Thomas, W. Zhang and M. E. Kordesh, *Nano Lett.*, 2006, **6**, 783–788.
149 H. H. Richardson, M. T. Carlson, P. J. Tandler, P. Hernandez and A. O. Govorov, *Nano Lett.*, 2009, **9**, 1139–1146.
150 A. G. Skirtach, C. Dejugnat, D. Braun, A. S. Susha, A. L. Rogach, W. J. Parak, H. Möhwald and G. B. Sukhorukov, *Nano Lett.*, 2005, **5**, 1371–1377.
151 M. Perner, J. Feldmann, S. Gresillon, J. März, G. Von Plessen, J. Porstendorfer, K.-J. Berg and G. Berg, *Phys. Rev. Lett.*, 2000, **85**, 792–795.
152 S. Link and M. A. El-Sayed, *J. Phys. Chem. B*, 1999, **103**, 8410–8426.
153 P. M. Bendix, S. N. S. Reihani and L. B. Oddershede, *ACS Nano*, 2010, **4**, 2256–2262.
154 H. Goldenberg, *Br. J. Appl. Phys.*, 1952, **3**, 296–298.
155 A. O. Govorov and H. H. Richardson, *Nano Today*, 2007, **2**, 30–38.
156 V. Kotaidis and A. Plech, *Appl. Phys. Lett.*, 2005, **87**, 213102.
157 V. Kotaidis, C. Dahmen, G. Von Plessen, F. Springer and A. Plech, *J. Chem. Phys.*, 2006, **124**, 184702.
158 A. Habenicht, M. Olapinski, F. Burmeister, P. Leiderer and J. Boneberg, *Science*, 2005, **309**, 2043–2045.
159 W. Huang, W. Qian and M. A. El-Sayed, *J. Am. Chem. Soc.*, 2006, **128**, 13330–13331.
160 G. V. Hartland, *Annu. Rev. Phys. Chem.*, 2006, **57**, 403–430.
161 G. V. Hartland, M. Hu, O. Wilson, P. Mulvaney and J. E. Sader, *J. Phys. Chem. B*, 2002, **106**, 743–747.
162 W. Huang, W. Qian and M. A. El-Sayed, *J. Phys. Chem. B*, 2005, **109**, 18881–18888.
163 D. Pissuwan, T. Niidome and M. B. Cortie, *J. Controlled Release*, 2009, **149**, 65–71.
164 L. Paasonen, T. Laaksonen, C. Johans, M. Yliperttula, K. Kontturi and A. Urtti, *J. Controlled Release*, 2007, **122**, 86–93.
165 S. J. Leung, T. S. Troutman and M. Romanowski, *Proceedings-Society of Photo-Optical Instrumentation Engineers*, NIH Public Access, 2009, **vol. 7190**, p. 7190.
166 L. J. E. Anderson, E. Hansen, E. Y. Lukianova-Hleb, J. H. Hafner and D. O. Lapotko, *J. Controlled Release*, 2010, **144**, 151–158.
167 J. L. West, S. R. Sershen, N. J. Halas, S. J. Oldenburg and R. D. Averitt, *J. Biomed. Mater. Res.*, 2000, **51**, 293–298.
168 J. L. West and N. J. Halas, *Curr. Opin. Biotechnol.*, 2000, **11**, 215–217.
169 B. Radt, T. A. Smith and F. Caruso, *Adv. Mater.*, 2004, **16**, 2184–2189.
170 A. G. Skirtach, C. Dejugnat, D. Braun, A. S. Susha, A. L. Rogach, W. J. Parak, H. Möhwald and G. B. Sukhorukov, *Nano Lett.*, 2005, **5**, 1371–1377.
171 G. B. Sukhorukov, A. L. Rogach, M. Garstka, S. Springer, W. J. Parak, O. Kreft, A. G. Skirtach, A. S. Susha, Y. Ramaye, R. Palankar and M. Winterhalter, *Small*, 2007, **3**, 944–955.
172 A. Barhoumi, R. Huschka, R. Bardhan, M. W. Knight and N. J. Halas, *Chem. Phys. Lett.*, 2009, **482**, 171–179.
173 R. Huschka, O. Neumann, A. Barhoumi and N. J. Halas, *Nano Lett.*, 2010, 4117–4122.
174 L. R. Hirsch, R. J. Stafford, J. A. Bankson, S. R. Sershen, B. Rivera, R. E. Price, J. D. Hazle, N. J. Halas and J. L. West, *Proc. Natl. Acad. Sci. U. S. A.*, 2003, **100**, 13549–13554.
175 X. Huang, I. H. El-Sayed, W. Qian and M. A. El-Sayed, *J. Am. Chem. Soc.*, 2006, **128**, 2115–2120.
176 M. Gobin, M. H. Lee, N. J. Halas, W. D. James, R. A. Drezek and J. L. West, *Nano Lett.*, 2007, **7**, 1929–1934.
177 X. Huang, S. Neretina and M. A. El-Sayed, *Adv. Mater.*, 2009, **21**, 4880–4910.
178 S. W. Hell, *Science*, 2007, **316**, 1153–1158.
179 C. Langhammer, E. M. Larsson, B. Kasemo and I. Zorić, *Nano Lett.*, 2010, **10**, 3529–3538.
180 A. S. Urban, M. Fedoruk, M. R. Horton, J. O. Rädler, F. D. Stefani and J. Feldmann, *Nano Lett.*, 2009, **9**, 2903–2908.
181 T. Numata, H. Tatsuta, Y. Morita, Y. Otani and M. Umeda, *IEEJ Trans. Electr. Electron. Eng.*, 2007, **2**, 398–401.


 

182 A. G. Skirtach, D. G. Kurth and H. Möhwald, *Appl. Phys. Lett.*, 2009, **94**, 093106.
183 J. R. Adleman, D. A. Boyd, D. G. Goodwin and D. Psaltis, *Nano Lett.*, 2009, **9**, 4417–4423.
184 L. Novotny, in *Topics in Applied Physics*, ed. S. Kawata, Springer Verlag, Berlin, 2000, **vol. 81**, pp. 123–141.
185 M. Nieto-Vesperinas, P. C. Chaumet and A. Rahmani, *Philos. Trans. R. Soc. London, Ser. A*, 2004, **362**, 719–737.
186 V. Yannopapas, *Phys. Rev. B: Condens. Matter Mater. Phys.*, 2008, **78**, 045412.
187 Z. Li, M. Käll and H. Xu, *Phys. Rev. B: Condens. Matter Mater. Phys.*, 2008, **77**, 1–6.
188 K. Svoboda and S. M. Block, *Opt. Lett.*, 1994, **19**, 930–932.
189 E. D. Palik, *Handbook of Optical Constants of Solids*, Academic Press, Boston, 1985.
190 J. R. Arias-González and M. Nieto-Vesperinas, *J. Opt. Soc. Am. A*, 2003, **20**, 1201–1209.
191 K. C. Toussaint, M. Liu, M. Pelton, J. Pesic, M. J. Guffey, P. Guyot-Sionnest and N. F. Scherer, *Opt. Express*, 2007, **15**, 12017–12029.
192 C. Selhuber-Unkel, I. Zins, O. Schubert, C. Sönnichsen and L. B. Oddershede, *Nano Lett.*, 2008, **8**, 2998–3003.
193 M. Pelton, M. Liu, H. Y. Kim, G. Smith, P. Guyot-Sionnest and N. F. Scherer, *Opt. Lett.*, 2006, **31**, 2075–2077.
194 P. M. Hansen, V. K. Bhatia, N. Harrit and L. Oddershede, *Nano Lett.*, 2005, **5**, 1937–1942.
195 T. Sugiura, T. Okada, Y. Inouye, O. Nakamura and S. Kawata, *Opt. Lett.*, 1997, **22**, 1663–1665.
196 M. Dienerowitz, M. Mazilu, P. J. Reece, T. F. Krauss and K. Dholakia, *Opt. Express*, 2008, **16**, 4991–4999.
197 Q. Zhan, *Opt. Express*, 2004, **12**, 3377–3382.
198 S. Kawata and T. Sugiura, *Opt. Lett.*, 1992, **17**, 772–774.
199 M. Lester and M. Nieto-Vesperinas, *Opt. Lett.*, 1999, **24**, 936–938.
200 F. Depasse and D. Courjon, *Opt. Commun.*, 1992, **87**, 79–83.
201 L. Novotny, R. Bian and X. Xie, *Phys. Rev. Lett.*, 1997, **79**, 645–648.
202 P. Chaumet, A. Rahmani and M. Nieto-Vesperinas, *Phys. Rev. Lett.*, 2002, **88**, 123601.
203 K. Okamoto and S. Kawata, *Phys. Rev. Lett.*, 1999, **83**, 4534–4537.
204 L. A. Blanco and M. Nieto-Vesperinas, *J. Opt. A: Pure Appl. Opt.*, 2007, **9**, S235–S238.
205 M. Righini, A. S. Zelenina, C. Girard and R. Quidant, *Nat. Phys.*, 2007, **3**, 477–480.
206 M. Righini, P. Ghenuche, S. Cherukulappurath, V. Myroshnychenko, F. J. García de Abajo and R. Quidant, *Nano Lett.*, 2009, **9**, 3387–3391.
207 A. N. Grigorenko, N. W. Roberts, M. R. Dickinson and Y. Zhang, *Nat. Photonics*, 2008, **2**, 365–370.
208 W. Zhang, L. Huang, C. Santschi and O. J. F. Martin, *Nano Lett.*, 2010, **10**, 1006–1011.
209 J. Prikulis, F. Svedberg, M. Käll, J. Enger, K. Ramser, M. Goksör and D. Hanstorp, *Nano Lett.*, 2004, **4**, 115–118.
210 F. Svedberg, Z. Li, H. Xu and M. Käll, *Nano Lett.*, 2006, **6**, 2639–2641.
211 Y. Jiang, T. Narushima and H. Okamoto, *Nat. Phys.*, 2010, **6**, 1–5.